The Resilience of Amazon Tree Cover to Past and Present Drying

Tyler Kukla[a,*], Anders Ahlström[b,c], S. Yoshi Maezumi[d], Manuel Chevalier[e,f], Zhengyao Lu[b], Matthew J. Winnick[g], C. Page Chamberlain[a]

[a] *Department of Geological Sciences, Stanford University, USA*
[b] *Department of Physical Geography and Ecosystem Science, Lund University, Sweden*
[c] *Center for Middle Eastern Studies, Lund University, Sweden*
[d] *Department of Ecosystem and Landscape Dynamics, University of Amsterdam, Netherlands*
[e] *Institut für Geowissenschaften und Meteorologie, Rheinische Friedrich-Wilhelms-Universität Bonn, Germany*
[f] *Institute of Earth Surface Dynamics, Geopolis, University of Lausanne, Switzerland*
[g] *Department of Geosciences, University of Massachusetts, Amherst, USA*

Abstract

The Amazon forest is increasingly vulnerable to dieback and encroachment of grasslands and agricultural fields. Threats to these forested ecosystems include drying, deforestation, and fire, but feedbacks among these make it difficult to determine their relative importance. Here, we reconstruct the central and western Amazon tree cover response to aridity and fire in the mid-Holocene—a time of less intensive human land use and markedly drier conditions than today—to assess the resilience of tree cover to drying and the strength of vegetation-climate feedbacks. We use pollen, charcoal, and speleothem oxygen isotope proxy data to show that Amazon tree cover in the mid-Holocene was resilient to drying in excess of the driest bias-corrected future precipitation projections. Experiments with a dynamic global vegetation model (LPJ-GUESS) suggest tree cover resilience may be owed to weak feedbacks that act to amplify tree cover loss with drying. We also compare these results to observational data and find that, under limited human interference, modern tree cover is likely similarly resilient to mid-Holocene levels of aridification. Our results suggest human-driven fire and deforestation likely

*Correspondence: T. Kukla, 450 Jane Stanford Way, Building 320 Stanford, CA 94305
Email address: tykukla@stanford.edu (Tyler Kukla)

Preprint submitted to Global and Planetary Change *May 7, 2021*

pose a greater threat to the future of Amazon ecosystems than drying alone.

Keywords: Amazon resilience, oxygen isotopes, pollen, fire, dynamic global vegetation model, mid-Holocene

1. Introduction

Ecological resilience is a measure of how much disturbance, or forcing, a system can absorb without changing its state [1, 2, 3]. The state of the system can be defined in a number of ways, but usually refers to its feedbacks and/or function [1, 2, 4]. Thus, ecological resilience (hereafter, resilience) is a useful concept for identifying the range of external conditions under which a system's behavior may vary, but its state does not fundamentally change.

As Amazon vegetation faces increasing ecological stress from climate change [5, 6, 7, 8, 9] and human development [10, 11, 12, 13, 7, 8, 9, 12, 13], the resilience of Amazon vegetation to external forcing becomes a central question surrounding the future of Amazon ecosystems. Amazon resilience can be understood from a wide range of perspectives depending on how the state of the system and its external forcings are defined. For example, some studies explore the resilience of biomass to future climate change, using biomass as the metric defining the state of the system and climate change to define the forcing [14, 15]. Other studies isolate the effect of water availability by examining the resilience of tree cover (the state of the system) to precipitation or drying (the forcing) [16, 17, 18, 19, 20].

Building on this extensive modern work, this study aims to characterize the resilience of central and western Amazon tree cover to drier, mid-Holocene ($\sim$ 6 ka) conditions [21, 22, 23, 24, 25, 26, 27, 28], and compare mid-Holocene tree cover resilience to the present. We stress that this approach cannot account for other dimensions of rainforest resilience, like species composition or diversity. Instead, we focus specifically on the resilience of tree cover to drying for three reasons. First, tree cover and precipitation can be reasonably inferred from paleo proxy data [21, 29, 30, 31, 32, 22]. Second, tree cover is a useful metric for comparing two alternative, well-defined states of Amazon vegetation—a high-tree cover forest and a low-tree cover savanna/grassland [18, 33]. Third, some modern data indicate that annual precipitation rates are near a “tipping-point” of 2,000 mm/yr, below which vegetation water-stress is enhanced along with feedbacks that may favor a forest-to-grassland transition [34, 35, 36]. If precipitation is near this tipping-point today, it is possible that the tipping point was crossed during drier times in the past.

The 2,000 mm/yr tipping point is ecologically meaningful because, across the tropics, it approximates a transition between a dry-season water surplus ($> 2,000$ mm/yr) and a dry-season water deficit ($< 2,000$ mm/yr) [36]. Below this threshold forests take more time to recover from a drought [37], dry-season photosynthesis declines, favoring deciduous and semi-deciduous vegetation [36, 38], and the wet season may grow shorter with a delayed onset, amplifying drying [39, 40, 41, 42, 43]. Further, both natural and human fires may increase under a dry-season water deficit. Fire correlates positively with the dry-season water deficit and negatively with relative humidity in Amazonia [44, 45] and seasonal aridity makes human-driven fire and deforestation easier in the dry season [45, 46, 47]. A seasonal water deficit and fire is often thought to favor grasslands in competition against forests because grasses generally recover faster from droughts and fires and they tend to be more flammable, inhibiting some tree growth [48, 49, 50, 51, 37, 45]. But could future aridity alone drive widespread forest dieback and grassland expansion in Amazonia?

Some models suggest that future climate change can devastate large swaths of Amazon tree cover [52, 53, 54, 5], but recent work has brought models and observations into agreement that Amazon tree cover may remain high despite future drying [35, 19, 20, 13]. Still, models and observations have their own limitations when unraveling the relationship between precipitation and tree cover. Models can simulate the effect of aridity in the absence of human deforestation [9] but the tree cover response to drying is highly sensitive to parameterizations [54, 55, 56, 35]. Observational datasets can be filtered to remove deforested sites [17, 19], but this can introduce biases associated with the spatial pattern of deforestation and does not account for non-local consequences of deforestation [57, 35, 58]. To circumvent these challenges, paleo-archives from times when human land use was less intensive are useful for exploring the relationship between precipitation and tree cover while limiting confounding factors.

Here, we test the hypothesis that Amazon tree cover is resilient to drying—specifically below the 2,000 mm/yr threshold—using the mid-Holocene as a case study. Existing data suggest that the central and western Amazon Rainforest remained largely intact with high tree cover in the mid-Holocene [59, 29, 21, 22]. However, the vast majority of precipitation proxy records have been interpreted qualitatively, so it is unclear whether high tree cover in the mid-Holocene is owed to high resilience to drying, or whether mid-Holocene proxies record only modest decreases in precipitation. We present a quantitative estimate for mid-Holocene precipitation based on speleothem oxygen isotope gradients and we compile pollen and charcoal proxy data to assess the relationship between precipitation, fire, and tree cover. We then test whether this relationship is supported in a dynamic global vegetation model (LPJ-GUESS v4.0 [60]) and we compare our results to modern precipitation and tree cover data. In doing so, we address two questions: 1) How resilient was mid-Holocene tree cover to drying? And 2) Is Amazon tree cover similarly resilient today?

2. A conceptual model for the tree cover response to external forcing and internal feedbacks

2.1. Conceptual model framework

Following previous work, we consider the state of the system in three groups based on the percent of area covered by trees: 1) a high tree cover state (>70%) to represent forests, 2) a low tree cover state (5-20%) to represent savannas or grasslands and 3) a transitional state at intermediate values [17, 18, 33]. We assess how the state of the system (forest, grass/savanna, or transitional) changes as a function of three forcings (precipitation, deforestation, and anthropogenic fire) and two positive feedbacks that arise from their interactions within the system. The Moisture Recycling Feedback (MRF) connects precipitation, tree cover, and evapotranspiration and illustrates how drying can decrease tree cover which, in turn, decreases evapotranspiration leading to further drying [58, 57, 35]. The second feedback includes the MRF loop and adds the effect of fire (MRF + Fire). In this case, a drop in precipitation increases natural fire which decreases tree cover and evapotranspiration, exacerbating the precipitation decline. The system is illustrated in Figure 1.

2.2. Tree cover response scenarios

The response of tree cover to precipitation depends on the relative contributions of forcings and feedbacks. Deforestation and anthropogenic fire, independent of any feedbacks, decrease tree cover without modifying precipitation (Fig. 2A, pink arrow). Changes in precipitation, independent of feedbacks, change tree cover when water limits primary productivity, following the “maximum potential tree cover” curve in Figure 2A.

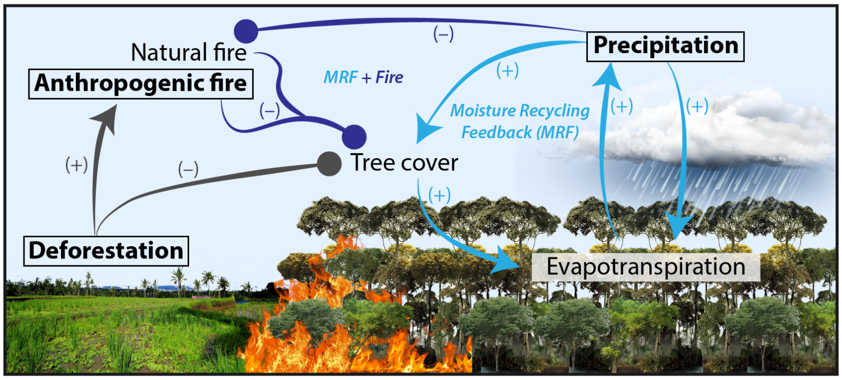

Figure 1: Schematic of forcings (boxes with bold font) and feedbacks (light and dark blue arrows) in our conceptual model. Tree cover defines the state of the model system. Arrows start at a cause and end at an effect with arrowheads denoting a positive relationship and closed circles denoting a negative relationship. The moisture recycling feedback (MRF) loop is shown in light blue arrows, and the contribution of fire (MRF + Fire) in dark blue. Deforestation and anthropogenic fire directly decrease tree cover (no feedback) and can indirectly decrease tree cover through the MRF and MRF + Fire feedbacks. A feedback in this diagram is positive if the sum of closed circles within a given loop is an odd number and negative if the sum is even.

Feedbacks in the system are considered stronger when changes in tree cover are larger for a given change in precipitation (proportional to the area of wedges in Fig. 2A). Thus, the feedback strength can change if the functional form of the precipitation-tree cover relationship changes (moving from one solid line to another in Fig. 2A) or if the initial precipitation rate changes (moving along a solid line in Fig. 2A). The MRF increases the distance the system moves along a given precipitation-tree cover curve for a given forcing. In this case, precipitation is still the only mechanism limiting tree cover in this feedback loop, so the sensitivity of tree cover to precipitation (the slope of the curve) remains a single function of precipitation. By contrast, increasing the sensitivity of fire to precipitation presents a new limit on tree cover and can push the state of the system to a new curve in precipitation-tree cover space (Fig. 2A, orange arrow). In our conceptual model the MRF + Fire loop is the only mechanism for abruptly "tipping" the state of the system (tree cover) without a proportional change in the forcing (i.e. by moving from one curve to another). The MRF without fire can lead to an abrupt change in tree cover but the forcing—precipitation—will change proportionately so it does not constitute tipping behavior.

The implication of our conceptual framework is that multiple stable states—the condition where more than one ecological regime is stable for a given precipitation rate—can only be driven by fire. This is supported by fire exclusion experiments around the world where closed forests replace grasslands without a large change in precipitation [61, 62, 63, 64, 65, 66] and by recent modeling work showing multiple stable states are absent from a dynamic global vegetation model unless fire-vegetation feedbacks are included [55].

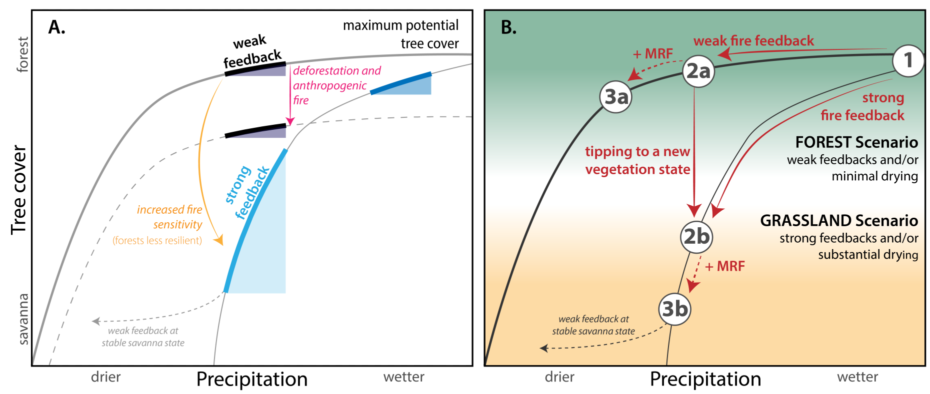

Figure 2: Multiple possible tree cover responses to precipitation based on the relevant forcings and feedbacks. (**A**) The strength of positive feedbacks is proportional to the area of wedges, and can vary by moving along a curve or switching between curves. (**B**) Different feedbacks have different effects on how tree cover changes with precipitation. Moving from point 1 to 2a or 2b shows how the fire feedback changes the slope of the tree cover-precipitation relationship (stronger feedback leads to a steeper slope). The MRF increases the distance the system moves along a curve. With the MRF the system can move from point 1 to 3a (3b) with the same forcing otherwise required to move to 2a (2b). If the positive fire feedback strengthens at some precipitation threshold the system can abruptly "tip" from point 2a to 2b. The transition from a forest to grassland thus requires strong, positive feedbacks and/or substantial drying.

Figure 2B shows how tree cover could change with time (from points 1 to 3) under different feedback scenarios. Beginning at point 1 with high precipitation and high tree cover, drying pushes the state of the system along a defined precipitation-tree cover trajectory from points 1 to 2. If the positive fire feedback is weak, tree cover will remain near the "maximum potential tree cover" line, ending at point 2a. If it is strong, the system moves along a steeper curve to point 2b. In contrast, the MRF increases the magnitude of change along a precipitation-tree cover curve. Thus, with a strong MRF the system will move from points 1 to 3 in the same time it would otherwise take to go from points 1 to 2 on its given trajectory (a or b). However, feedback strength is often also a function of precipitation. For example, the fire feedback is likely weak/strong when precipitation rates (and humidity) are high/low, respectively [61, 67, 44]. If the fire feedback abruptly strengthens at some precipitation threshold, it can "tip" the system from a forest to grassland state. This is depicted in the path from points 2a to 2b where strengthening of the fire feedback at point 2a causes the system to "tip" to point 2b (Fig. 2B).

Using this conceptual model with proxy data for fire, vegetation, and precipitation we can infer the strength of the different forcings and feedbacks by reconstructing the history of tree cover and precipitation. To illustrate this, consider a decrease in precipitation from point 1 to points 2a and 2b (Fig. 2B). In order to maintain a forest despite drying, positive feedbacks and anthropogenic forcing must be weak. But a transition to a grassland state indicates that anthropogenic forcing is strong, positive feedbacks are strong, and/or positive feedbacks strengthened within the range of drying causing the system to "tip". Proxy records can then be used to determine which of these options is most likely by indicating, for example, how sensitive fire is to drying.

3. The Amazon Basin in the mid-Holocene

3.1. Mid-Holocene proxy records

The mid-Holocene ($\sim$ 6ka) is an ideal period to evaluate the Amazon tree cover response to aridification because it is associated with widespread proxy data indicating one of the driest times of the late Quaternary [21, 68, 25, 69, 70]. While the onset of drier conditions varies from the early to mid-Holocene depending on the location, drier conditions generally lasted through, and often peaked at, 6 ka [24, 71, 72, 73, 70, 22]. Drying is especially pronounced in the central, western, and southwestern Amazon and drier conditions are also observed on a continental scale in offshore records of terrestrial runoff [26, 27, 28, 74, 75] (Fig. 3A). This coincides with the desiccation of lakes and fluvial systems in the western Andean plateau [24, 23, 76, 25, 77] and local-to-regional increases in savanna coverage and fire [29, 21] (Fig. 3A), particularly in the southwestern Amazon. While patches of savanna expanded within the forested regions of southwestern Amazon at this time [78, 69], the central and western Amazon domain, or core rainforest region (Fig. 3B, inset), likely remained intact [29, 21, 59, 22].

In addition to climate, humans may have also played a role in modifying Amazon vegetation in the mid-Holocene. Human settlements were extensive in the mid-Holocene, spanning much of southwestern Amazonia with evidence for cultivation and food production [79, 80, 81, 82, 83]. Some evidence suggests human populations declined in the mid-Holocene [84], but this signal may be related to geomorphic or sampling biases [85]. Despite the broad spatial coverage of human settlement in the mid-Holocene, land use and human-driven vegetation change was more localized and less intensive than today. Many human settlements took advantage of naturally open vegetation rather than creating space through widespread clear-cutting [81, 85]. Further, at least in the late Holocene the climate-driven expansion of rainforest around human settlements provides evidence for sustainable land management practices that did not interfere with regional-scale climate-vegetation relationships [86, 81]. Thus, while human occupation was extensively distributed across some parts of the basin during the mid-Holocene, climate most likely remained the primary control on regional tree cover with human land use occurring on a smaller scale than today.

Our compiled proxy data includes charcoal and pollen records, along with speleothem oxygen isotope data from sites spanning the central and western Amazon (Fig. 3B). We also compare to a variety of proxy types used to reconstruct mid-Holocene vegetation in Smith and Mayle, 2018 [21]. We align our proxy data with the isotope gradient in order to directly compare precipitation, tree cover, and fire, but most available pollen and charcoal records are in the western Amazon and we lack uniform coverage across the central basin. Here, the assorted proxy records of Smith and Mayle [21] help compensate for a paucity of pollen and charcoal data. Some records to the north approach regions where previous studies have interpreted wet mid-Holocene conditions (3A), and this may also bias our results. However, we repeat our analysis with southwestern Amazon pollen and charcoal records, where proxy data reveal more uniform drying, and find that this sampling bias does not affect our conclusions (Supplemental Fig. S1).

3.2. Mid-Holocene climate

Amazon precipitation in the late Quaternary is thought to follow a zonal dipole pattern, with anomalous precipitation shifts between the eastern and western/southwestern basin on precessional and glacial-interglacial timescales [31, 87, 32, 88, 89, 90]. During the mid-Holocene, data suggest the dipole was likely in its “eastern phase” with positive anomalous precipitation over

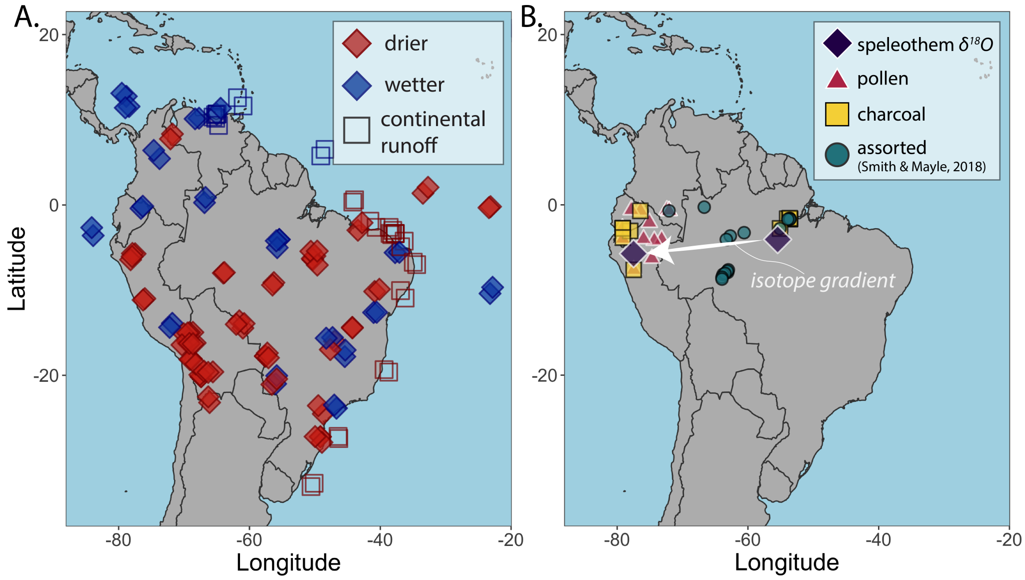

Figure 3: (**A**) Proxy compilation for the mid-Holocene (defined here as 5-7 ka). See Supplementary data for full reference list. Blue points represent a proxy indicating wet or wetter conditions and red points are drier. Diamonds are local/regional proxies and open squares are marine core records of continental runoff. (**B**) Map of the pollen (magenta triangles), charcoal (yellow squares) and speleothem $\delta^{18}O$ (purple diamonds) records used in this study. Teal circles show proxy records of assorted type from Smith and Mayle, 2018 [21] that fall within our domain.

eastern Amazonia and NE Brazil [31, 87]. The mechanism for precipitation dipole transitions remains debated, but it is usually linked to the strength of the South American Monsoon with the eastern phase occurring during a weaker monsoon [31, 32, 91, 92].

In addition to dynamic changes in the spatial pattern of moisture convergence, Amazon precipitation is also sensitive to how moisture is recycled across the basin. Today and in the mid-Holocene the central and western Amazon sits inland from the primary moisture source—the easterly trade winds that cross the Atlantic Ocean [93, 94]—so precipitation is strongly dependent on upstream moisture recycling. About one-third to half of all precipitation in this region is derived from evapotranspiration within the basin today [58, 57, 95, 96], making it particularly sensitive to feedbacks like the MRF that can promote forest-grassland transitions [42, 97, 58, 57, 35, 98, 47]. If feedbacks like the MRF can promote forest-grassland transitions, the western Amazon is an ideal place to detect this signal.

4. Methods

4.1. Oxygen isotope gradient and precipitation reconstruction

4.1.1. Isotope gradient reconstruction and the importance of the "hydrostat"

Oxygen isotopes in calcite cave deposits, or speleothems, can reflect the isotopic composition of past rainfall and provide useful information for reconstructing monsoon dynamics [99, 31, 30, 100, 101, 32, 102]. We use the change in Amazon speleothem $\delta^{18}O$ over space—the isotope gradient($\Delta\delta^{18}O$; ‰/1,000km)—with a reactive transport model [103, 104, 105, 106] to solve for precipitation rates. This is done by reconstructing past isotope gradients along the South American Monsoon moisture trajectory with $\delta^{18}O$ records from three sites—one in east-central Amazon [30] and two that form a composite record in the western Amazon [32, 102] (Fig. 4). We also adopt the $\delta^{18}O$ correction that accounts for differential cave temperatures between the sites previously used in references [30, 107].

The isotope gradient is useful because it reflects changes in the regional water balance while limiting the influence of confounding factors. The balance of precipitation (P) and evapotranspiration (ET) across a moisture trajectory sets the isotope gradient because P tends to decrease $\delta^{18}O$ by removing moisture from an air mass while ET increases $\delta^{18}O$ by replenishing the air mass [108]. Thus, $\Delta\delta^{18}O$ decreases as P increases relative to ET. Additional effects unrelated to the water balance, like upstream effects and temperature, can influence $\delta^{18}O$ at a single site, but isotope gradients are insensitive to these factors because they do not modify the rainout-recycling balance [103, 104, 109]. As a result, the isotope gradient across Amazonia has long been used as a metric for the balance of P and ET [108].

Importantly, the oxygen isotope gradient (along with $\delta^{18}O$ at a given point) is not always sensitive to precipitation rates [106, 110, 103]. As P decreases, the isotope gradient shallows until it asymptotes at the theoretical maximum value of zero (meaning there is no change in $\delta^{18}O$ between the upstream and downstream sites). The point where the isotope gradient reaches zero is called the "hydrostat"—the condition where further aridification will have no affect on $\Delta\delta^{18}O$ values [106, 110, 103]. The hydrostat is reached because the net distillation of moisture is near zero as climatological rates of P and ET are nearly equal. This can occur when P rates are similar to or below potential evapotranspiration (E_0) rates. Since E_0 is an upper limit on ET, P must exceed ET when $P > E_0$, leading to a decrease in $\delta^{18}O$ and a negative P-$\delta^{18}O$ relationship known as the "amount effect" [111, 103, 112, 113, 114, 115]. Therefore, when $\Delta\delta^{18}O$ is near zero it is possible to constrain the upper bound of precipitation rates—the point where P exceeds potential ET—but not the lower bound.

4.1.2. Reconstructing past mean annual rainfall

We use the reactive transport model (RTM) [103], which simulates atmospheric vapor transport (w), rainout (P), and evapotranspiration (ET), to inversely solve for mid-Holocene rainfall rates from speleothem $\Delta\delta^{18}O$ data. We initialize the model with distributions of the source moisture content (similar to specific humidity), potential evapotranspiration, surface temperature, the wind speed profile, evapotranspiration partitioning, a moisture recycling efficiency parameter, and a vapor condensation rate constant. Sampling from these input distributions $> 50,000$ times, the model solves for the spatial pattern of precipitation and evapotranspiration as well as the oxygen isotope ratios of these fluxes [103]. See Supplemental Text S1 for further information on model initialization.

Using the results of our Monte Carlo routine we calculate the mean rainfall consistent with the observed $\Delta\delta^{18}O$ to produce a mean annual rainfall distribution. During the mid-Holocene, $\Delta\delta^{18}O$ values fall along the hydrostat and the RTM loses sensitivity to the lower bound of rainfall (while the upper bound is still constrained). In order to extract a rainfall distribution in this case we impose a lower bound, thus assuming that any rainfall value below the imposed threshold is unreasonable. To develop a conservative estimate of mid-Holocene aridification we exclude any iteration where mean annual rainfall drops below half the potential evapotranspiration rate, a point at which modern tree cover is mostly below 50% (*e.g.* [36, 19]). We test the sensitivity of our results to this assumption with a range of thresholds (Supplemental Fig. S2) and find that this decision influences the mean rainfall value but does not affect our conclusions.

Our analysis implicitly assumes that moisture is transported directly from the eastern (upstream) speleothem site to the western sites. While this trajectory aligns well with the direction of the easterly trade winds (especially during the wet season) it is reasonable to expect that the effective moisture transport distance between these sites may have differed in the mid-Holocene due to changes in atmospheric circulation patterns. However, because $\Delta\delta^{18}O$ is near zero at the mid-Holocene the isotope gradient (and, thus, our results) are not sensitive to changes in assumptions about the effective moisture transport distance (Supplemental Fig. S3).

4.2. Pollen compilation

Twenty-three terrestrial pollen records were extracted from the Neotoma Paleoecology Database [116] and the ACER pollen and charcoal database [117] in March, 2020 across our study area (with data spanning 55° - 80°W and 8°S - 0°N; see Fig. 3B). Pollen percentages for all records were calculated based on the sum of terrestrial pollen taxa only (the pollen taxa classified as 'Tree/Shrub', 'Succulent', 'Upland herbs' and 'Palms' in Neotoma). Pollen samples were subsequently grouped into 200-year bins, which corresponds with the average resolution of the selected records (197 years between consecutive samples, on average), to extract a regional signal. The average bin size is 22.4 pollen samples with a range of 2-86 samples. For each bin, we calculate the ratio of arboreal (Tree and Shrubs, Palms) to non-arboreal (Herbs and Succulents) pollen taxa. While the classification of pollen taxa into unique vegetation forms contains some inaccuracies (*i.e.* all the species producing a pollen morphotype may not all belong to the same vegetation form), the associated uncertainties are expected to only have a negligible impact and/or compensate each other in our broad-scale, multi-site reconstruction.

4.3. Charcoal compilation

Charcoal records are compiled from the Global Charcoal Database (GCD version 2.0) and other published datasets. Charcoal data were analyzed using the paleofire R package software (version 1.1.8) [118]. Eleven charcoal records spanning 53° - 80°W and 8°S - 0°N are included in this analysis to create a regional charcoal curve (Supplemental Data, Fig. 4C). These sites provide an average of regional biomass burning during the Holocene. To facilitate inter-site comparison, the eleven records are pre-treated using a standard protocol [119, 120] for transforming and standardizing individual records that includes: (*1*) transforming non-influx data (*e.g.* concentration particles cm^{-3}) to influx values (particle cm^{-2}/yr), (*2*) homogenizing the variance using the Box-Cox transformation, (*3*) rescaling the values using a minimax transformation to allow comparisons among sites, and (*4*) rescaling the values to z-scores using a base period of 200 years. Sites are smoothed with a 500-year half width smoothing window and a bootstrap of 200 years [118].

4.4. Dynamic global vegetation modeling

To evaluate the mid-Holocene precipitation-tree cover relationship inferred from proxies while accounting for changes in other climate variables we conducted simulations with the second generation dynamic global vegetation model (DGVM) LPJ-GUESS [60, 121]. The simulated vegetation states emerge as an outcome of simulated vegetation structure, demography, resource competition for light, water and nutrients, and wild fires. Vegetation is represented as a mixture of plant functional types (PFTs) (11 in this study) [122], distinguished by photosynthetic pathway (C3 or C4), life history strategy (shade tolerance), phenology (evergreen, summergreen or raingreen), growth form (trees or herbaceous plants) and bioclimatic distributional limits.

LPJ-GUESS incorporates a fire model to link the fire regime and its effects on vegetation dynamics and biogeochemical cycling [123]. Fires are modelled prognostically based on temperature, current fuel load, and moisture. Daily litter moisture is used to estimate the fire season length which, in turn, determines the fraction of a grid cell that is burnt in a year. The relationships between litter moisture, fire season length, and burnt area are calibrated with modern data [123]. Fire return intervals are simulated by the model based on the yearly burnt area fraction. When driven by 20th century climate data, the simulated fire return intervals are in good agreement with observations in the Amazon and globally [123]. Since observational data for model calibration are assumed to be the most representative for natural conditions, human-changed fire regimes and other land use impacts are not explicitly considered, but could still have an effect on the final model processes [123].

Climate forcing (temperature, precipitation and radiation) of the offline LPJ-GUESS simulations comes from output of the coupled global climate model, EC-Earth [124]. The mid-Holocene orbital parameters and greenhouse gas concentration were prescribed for the standard mid-Holocene EC-Earth simulation (MH), while boundary conditions such as a vegetated Sahara and reduced dust aerosol (MHgsrd) were further added to a sensitivity simulation to reproduce a climate regime more consistent with proxy reconstructions [125]. The vegetation response in North Africa in these simulations was investigated in detail in a previous study [126]. In total, we performed six simulations. Three simulations—one pre-industrial (PI) and two mid-Holocene (MH, MHgsrd)—were forced with unperturbed climate forcing from EC-Earth and three simulations included further precipitation reductions. Amazon annual precipitation in the unperturbed simulations is

2,175, 2,002, and 1,776 mm/year for PI, MH, and MHgsrd. The precipitation reduction experiments use MHgsrd boundary conditions with annual precipitation reduced to 1,520, 1,420 and 1,260 mm/year. We compare our precipitation reduction experiments to MHgsrd in Fig. 6, but all results can be found in Supplemental Fig. S4 and S5.

Precipitation reductions were applied with a multiplier to scale average precipitation in the proxy region of Fig. 3B to the desired level. All grid cells (inside or outside the proxy domain) were multiplied by the same factor. Therefore, we restrict our analysis to the vegetation patterns within the proxy domain to avoid regions where precipitation scaling is unrealistic and outside the domain of $\Delta\delta^{18}O$ constraints. We also exclude the Andes to avoid a confounding, Andean taxa signal. To understand the role of fire disturbance, the 1,520 and 1,260 mm/year simulations were repeated with the fire module disabled (purple squares in Fig. 7). All LPJ-GUESS simulations were spun-up from bareground and run for 500-years to reach an equilibrium state. We use the last 10 years of output for analysis. Further information about our LPJ-GUESS simulations can be found in the Supplementary Text (S2).

4.5. Modern tree cover and precipitation data

We compile modern data for tree cover, precipitation, and human land use in order to compare past and DGVM-simulated estimates of tree cover and precipitation to modern conditions. Tree cover, precipitation, and land use data were compiled in ref [19]. Tree cover was collected from Landsat remote sensing data at 30m spatial resolution [127] with trees defined as being greater than 5m tall. Mean annual precipitation rates were calculated from the Global Precipitation Climatology Centre (GPCCv7) [128] using the correction of ref [129] for the years 1993-2012. Land use data are derived from ref [130].

5. Results

5.1. Oxygen isotope gradient reconstruction

The kernel smoothed oxygen isotope gradient values range from -1.3 to 0.1 ‰/1,000 km through the Holocene. The record plateaus and hovers around the hydrostat, the theoretical maximum isotope gradient [103, 106], from $\sim 11-5$ ka, before decreasing toward its lowest values in the present (Fig. 4A). The oxygen isotope gradient in modern precipitation across the

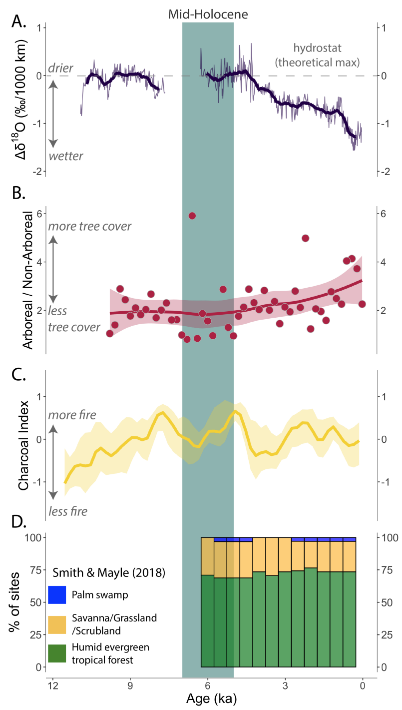

Figure 4: Proxy timeseries data. (**A**) The oxygen isotope gradient between the two speleothem sites. Darker curve is a kernel smooth through the data. (**B**) The ratio of arboreal to non-arboreal pollen. Line is a kernel smooth through the data. (**C**) The charcoal index timeseries (yellow line) with 95% confidence intervals shown by the translucent, yellow ribbon. (**D**) Percent of sites recording different vegetation types (from compilation of Smith and Mayle, 2018 [21].

Amazon is $\sim -1‰/1{,}000$ km [108, 103], similar to the gradient from the most recent speleothem $\delta^{18}O$ data.

While $\Delta\delta^{18}O$ values are stable near zero for much of the early-to-middle Holocene, independent proxy evidence from western Amazonia indicates precipitation was decreasing during this time [24, 23, 68, 131, 77, 76, 132]. Thus, the $\Delta\delta^{18}O$ record may not fully reflect the trends in precipitation through the Holocene due to $\Delta\delta^{18}O$ being insensitive to precipitation at the hydrostat.

5.2. Vegetation in the mid-Holocene

In western Amazonia the arboreal to non-arboreal pollen ratio ranges from 0.8 to 5.9 throughout the Holocene. Kernel smoothing of the data shows gradual increase in this ratio from $\sim$5 ka to present, mirroring a shift to lower $\Delta\delta^{18}O$ values. There is a weak, negative correlation between the ratio of arboreal to non-arboreal pollen and the oxygen isotope gradient (Supplemental Fig. S6). Some of the lowest arboreal/non-arboreal pollen ratios occur in the mid-Holocene, suggesting the possibility of some savanna expansion. We note that the arboreal/non-arboreal pollen ratio is not necessarily a reliable indicator of tree cover [133] and therefore we use it only to infer relative trends. Data from Smith and Mayle, 2018 [21] show that, from 6 ka to present, between 69 to 76% of sites in our proxy domain record humid evergreen tropical forest conditions, consistent with the rainforest remaining intact [29, 21, 59] (Fig. 4D).

5.3. Fire in the mid-Holocene

Our composite charcoal record shows a progressive increase of the charcoal index from -1 to 0.6 between 12 ka and 10 ka (Fig. 4C). Fire activity declines to a local minimum with a charcoal index of 0 around 6 ka, followed by a sharp increase to 0.7 around 5 ka. Another local minimum occurs around 3.5 ka, after which charcoal index values remain just above zero until present (Fig. 4C). The charcoal index is not significantly correlated with $\Delta\delta^{18}O$ nor the arboreal/non-arboreal pollen ratio (Supplemental Fig. S6). Despite the lack of correlation, fire may still be responsive to vegetation if it tracks changes in species composition, which may not vary with the arboreal/non-arboreal pollen ratio. Further, in contrast to our charcoal index curve, tropical glacier proxy records from the southwest, outside of our domain, indicate increased fire activity during the mid-Holocene [134, 135]. However, it is unclear whether this discrepancy with our composite record is owed to greater aridity in the southwest, a difference in vegetation composition, or something else.

5.4. RTM modeling and rainfall reconstruction

Our RTM results for the pre-industrial show modeled rainfall rates that are consistent with distributions from GPCC data [128] (Fig. 5). Inverting on the isotope gradient from the most recent speleothem $\delta^{18}O$ values yields a domain-mean rainfall estimate of 2,300 +/- 500 mm/yr, comparable to modern (2,480 +/- 470 mm/yr; Fig. 5). This builds on previous work indicating that spatial isotope gradients record information about climatological moisture fluxes [108, 109, 103, 104, 106].

Our mid-Holocene results indicate substantially drier conditions compared to the pre-industrial. In the mid-Holocene we estimate a rainfall rate

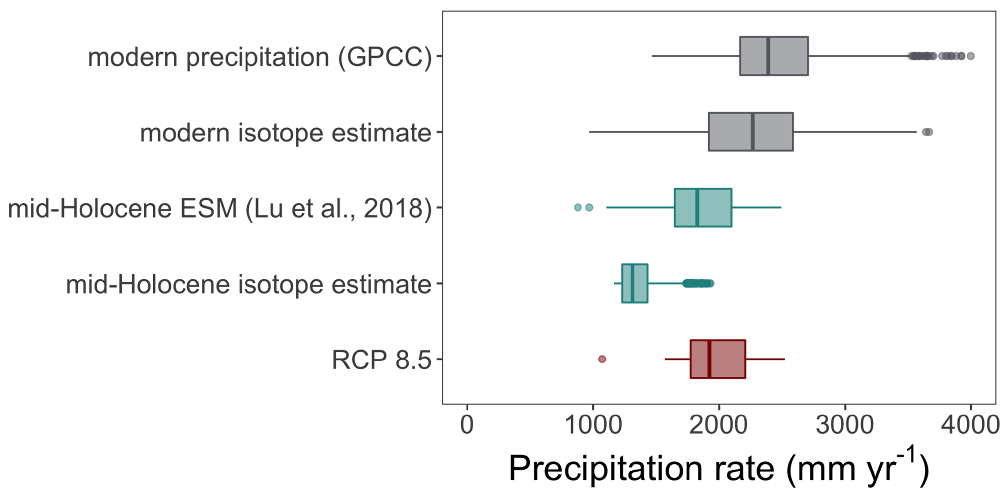

Figure 5: Precipitation distributions (from top to bottom) of: modern precipitation from the proxy domain from GPCCv7 [128], pre-Industrial precipitation estimate from the RTM inversion of the most recent speleothem $\Delta\delta^{18}O$ data, mid-Holocene precipitation in the proxy domain from the Green-Sahara simulations of ref [126], the wettest quarter of precipitation estimates from the RTM inversion on the mid-Holocene hydrostat $\Delta\delta^{18}O$ values, and estimates for future Amazon precipitation in RCP 8.5 from ref [19].

of ~1,300 mm/yr (Fig. 5), about 45% lower than present. This estimate is based on the wettest 25% of RTM iterations above the imposed lower-bound. We find no possible solutions exceeding 2,000 mm/yr and the maximum simulated precipitation rate is ~1,900 mm/yr. Despite the loss of model leverage at low precipitation rates, the exercise provides a valuable upper-bound on mean annual precipitation.

Our results demonstrate that mid-Holocene precipitation rates are likely substantially lower than most end-of-century precipitation estimates from simulations of unabated carbon emissions (RCP 8.5; Fig. 5). On average, models predict precipitation by the year 2100 will be ~ 400 mm/yr less than today with over half the models predicting future rainfall below the 2,000 mm/yr threshold. However, when accounting for model precipitation bias (usually a dry-bias in Amazonia) the mean change in future precipitation is much smaller—~26 mm/yr—with no models falling below 2,000 mm/yr. Since our mid-Holocene precipitation distribution does not exceed ~1,900 mm/yr, the lowest bias-corrected future estimate is greater than our highest estimates of mid-Holocene precipitation (Supplemental Fig. S7).

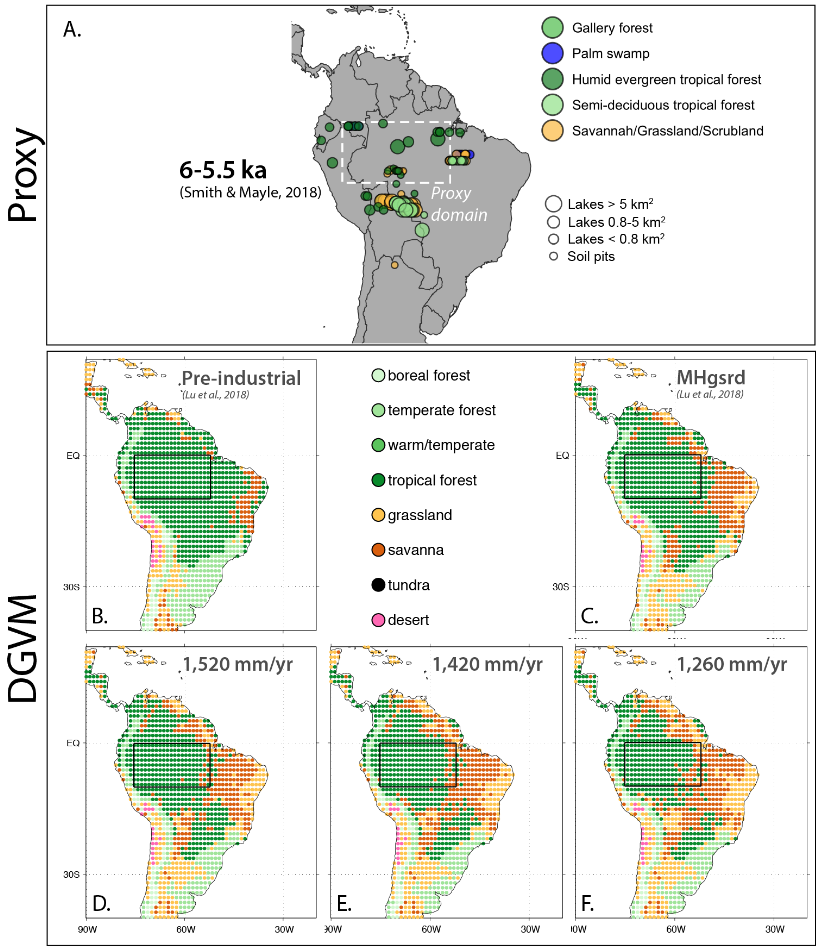

Figure 6: Dynamic global vegetation model results and comparison with comprehensive proxy compilation of ref [21]. (**A**) Proxy-derived biomes from the 6-5.5 ka timeslice of Smith & Mayle (2018) [21]. Sites with two major biomes are given two, jittered data points. Southwestern proxy region [21] is included for comparison with DGVM. (**B-F**) Results of DGVM simulations when precipitation is set to the simulations of ref [126] (pre-Industrial and mid-Holocene in **B, C**) or scaled to 1,520, 1,420, or 1,260 mm/yr within the proxy domain (black boxes) (**D-F**). Extensive savanna expansion in northeastern Brazil in panels *D-F* is likely unrealistic because it is outside the proxy domain and does not account for possible wetter conditions in this region in the mid-Holocene [31, 91, 87, 136].

5.5. Dynamic global vegetation model response to mid-Holocene rainfall

Tree cover in the core rainforest region (central and western Amazonia) remains intact in our DGVM simulations in a wide range of mean annual precipitation conditions (Fig. 6B-F) [126]. Turning off fire in our simulations leads to substantial increases in tree cover outside of the proxy domain (Supplemental Fig. S4) but has little effect within the domain (Fig. 7; Supplemental Fig. S8). This suggests that fire is effective at promoting grassland and savanna expansion near the forest fringes (ecotones) in the model, but may not lead to vast tree cover loss in the core forest regions. Most of the savanna and grassland expansion in the southwestern Amazon is inhibited in simulations where fire is turned off, suggesting that drying alone is not sufficient to drive large changes in tree cover within the range of precipitation rates simulated here.

Within the proxy domain tree cover remains at forested levels ($> 70\%$) at all precipitation rates whether fire is enabled or not (Fig. 7). Tree cover decreases from $\sim 92\%$ when precipitation is $\sim 2,200$ mm/yr to $\sim 80\%$ when precipitation drops to $\sim 1,300$ mm/yr. Disabling fire leads to an increase in tree cover of $\sim 4-5\%$ in the range of precipitation rates we tested. While our precipitation estimates span the range where forests and savanna are thought to reflect alternative stable states (the "bistability range" of 1,300-2,100 mm/yr [17]) we do not observe any marked shift to a savanna vegetation state in our simulations.

6. Discussion

6.1. Strength of mid-Holocene forcings and feedbacks

High tree cover in the mid-Holocene supports the hypothesis that central and western Amazon tree cover is resilient to crossing below the 2,000 mm/yr precipitation threshold, at least down to ~1,300 mm/yr. Here, we explore why tree cover might be so resilient. We compare the mid-Holocene estimates to the modern precipitation-tree cover relationship to construct an aridification trajectory that defines a tree cover response to drying. Using the proxy records in our conceptual model framework (Section 2), we infer the contributions of forcings and feedbacks from the trajectory. We note that precipitation-tree cover relationships have been theorized to follow a "hysteresis" pattern where the direction of change (wetting or drying) can determine the tree cover response [16]. This does not invalidate our approach of looking back in time to infer a forward aridification trajectory for two reasons. First, forests prevail in the core of Amazonia in the mid-Holocene through today [29, 59, 21] and hysteresis should only arise when the state of the system changes (*i.e.* forest to savanna or grassland). Second tree cover and precipitation were both higher prior to the Holocene [24, 23, 76, 131, 29, 27, 137, 28], so the modern conditions can also approximate an initial state for Holocene aridification.

Our precipitation constraints and existing vegetation reconstructions [29, 21, 59, 22] are supported by our DGVM simulations showing forest tree cover is maintained as precipitation reaches mid-Holocene levels (Fig. 7). This result is consistent with the forest scenario of Figure 2B. In this scenario, tree cover is near the maximum potential tree cover curve (gray line of Fig. 7) and precipitation is the dominant forcing on the system. High tree cover is maintained in this scenario as human forcing and the feedbacks that amplify tree cover loss (like the MRF and MRF + Fire) are not strong enough to change the state of the system.

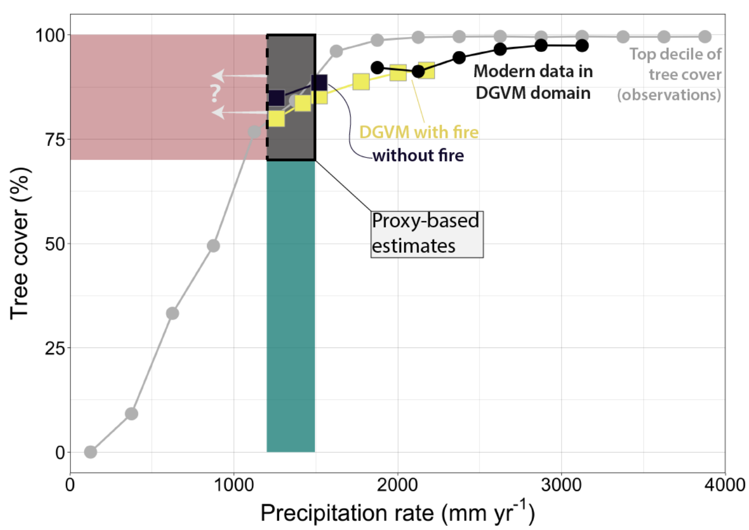

Figure 7: Modeled and proxy-based estimates for fire, precipitation, and tree cover dynamics in the mid-Holocene. Gray circles show the top decile of tree cover observations for each precipitation bin as an estimate of maximum potential tree cover. Black circles show tree cover and precipitation in the proxy domain (see Fig. 6A). Squares show DGVM output with fire (yellow) and without (purple) within the proxy domain. Proxy-based precipitation and tree cover estimates are shown in teal and red rectangles (region of overlap is boxed in black). Overall, observations, models, and proxy data agree that tree cover remains high at $\sim 1,300$ mm/yr of precipitation with no tipping to a grassland state.

Indeed, proxy estimates support, at most, a minor role for human forcing (deforestation) and fire in determining the state of Amazon tree cover in the central and western basin [138, 81, 80, 29, 86, 85]. Our charcoal index composite (which integrates anthropogenic and natural fire) does not show consistent trends with arboreal pollen or precipitation in the Holocene (Fig. 4; Supplemental Fig. S6). While this suggests fire is not strongly responsive to climate, we note the possibility that a long-term link between precipitation (Fig. 4A) and natural fire (Fig. 4C) might be overprinted by opposing trends in anthropogenic fire [84, 29, 139]. In either case, these proxy data suggest that human-driven fire forcing, natural fire feedbacks, or both, are too weak to drive grassland expansion in our proxy domain in the mid-Holocene.

Grassland and fire expansion, however, may have occurred near forest-savanna boundaries (or ecotones) in the mid-Holocene. Consistent with our DGVM results, most proxy evidence for grassland and fire expansion is restricted to ecotones [29, 21] while central and western Amazon records [21, 22] and basin-integrated records [59, 138] show little-to-no change through the mid-Holocene. This distinction between ecotonal and basin-integrated records suggests that fire and savanna expansion in ecotonal regions is a small portion of the basin mean, or their expansion is balanced by decreases in fire and grass coverage elsewhere. Fire plays an important role in ecotone migration in our DGVM simulations but this effect occurs mostly outside our proxy domain where our precipitation scaling is not constrained by proxy data (Supplemental Fig. S4). Within our proxy domain, however, the fire feedback in our DGVM simulations is weak and the tree cover response to drying is similar whether the fire module is enabled or disabled (Fig. 7). Overall, DGVM results are consistent with the finding that mid-Holocene fires were limited to forest-grassland ecotones and did not cause the system to tip to a savanna state. The fire feedback may have been strong in ecotonal regions, but it was weak in the core forested region where high tree cover persisted.

6.2. A seasonal water deficit in the mid-Holocene

The survival of Amazon forests and the passive nature of feedbacks that promote tree cover loss in our analysis is remarkable when we consider the consequences of mid-Holocene water stress. Today, regions of tropical South America that receive less precipitation than 2,000 mm/yr are vulnerable to seasonal water deficits [36]. Below this threshold more water is lost to evapotranspiration and runoff in the dry season than can be replenished by wet season water storage. The 2,000 mm/yr threshold should also apply in the mid-Holocene because it is set by the balance of potential evapotranspiration and water storage [36] and potential evapotranspiration scales weakly with temperature in the tropics (∼1.5%/K) [140]. Based on our precipitation estimates, it is likely that the central and western Amazon was affected by a seasonal water deficit in the mid-Holocene. Such a deficit would probably have an outsized effect on evergreen taxa that rely on stored water for dry season photosynthesis, while favoring seasonally dry forest taxa and grasses [36, 38, 37].

A seasonal water deficit can also amplify fire occurrence and lengthen the dry season in Amazonia. Fires have have been shown to increase exponentially with drying [44, 45] but the lack of a correlation between $\Delta\delta^{18}O$ and fire across the mid-Holocene suggests that dry season aridity does not increase fire sufficiently to drive widespread forest dieback. Meanwhile, under a water surplus in the dry season, transpiration of stored water acts as a "moisture pump" that prompts the onset of deep wet season convection 2-3 months before the peak shift in wind patterns associated with southward ITCZ migration [43]. If seasonal drying made it difficult for deep-rooted trees to access water and transpire, the onset of the wet season may have been substantially delayed in the mid-Holocene [39, 40, 41, 43, 42]

The consequences of seasonal aridity characterize the 2,000 mm/yr threshold as a possible "tipping" point where Amazon forests can be abruptly replaced by grasslands [37, 17, 18]. We cannot confirm whether the Amazon experienced a delayed onset of the wet season in the mid-Holocene, or whether climate-driven fire occurrence increased. But our results suggest that either (*1*) Amazon tree cover is resilient to the consequences of a seasonal water deficit or (*2*) the seasonal water deficit did not increase fire nor dry season length enough to tip the central/western Amazon to a grassland/savanna state.

6.3. Modern tree cover resilience compared to the mid-Holocene

Modern spatial data indicate that when mean annual precipitation falls between 2,100 mm/yr and 1,300 mm/yr forests and savannas are both stable ecological states [17, 18, 33]. This is referred to as the region of "bistability" within which a forest ecosystem can abruptly tip to a savanna state. Our mid-Holocene precipitation estimates suggest that even at the lower bound of this bistability region tree cover did not tip to a savanna state. Does forest survival in this range indicate drying alone is unlikely to lead to tipping today? Or is modern Amazon tree cover less resilient to drying than it was in the mid-Holocene?

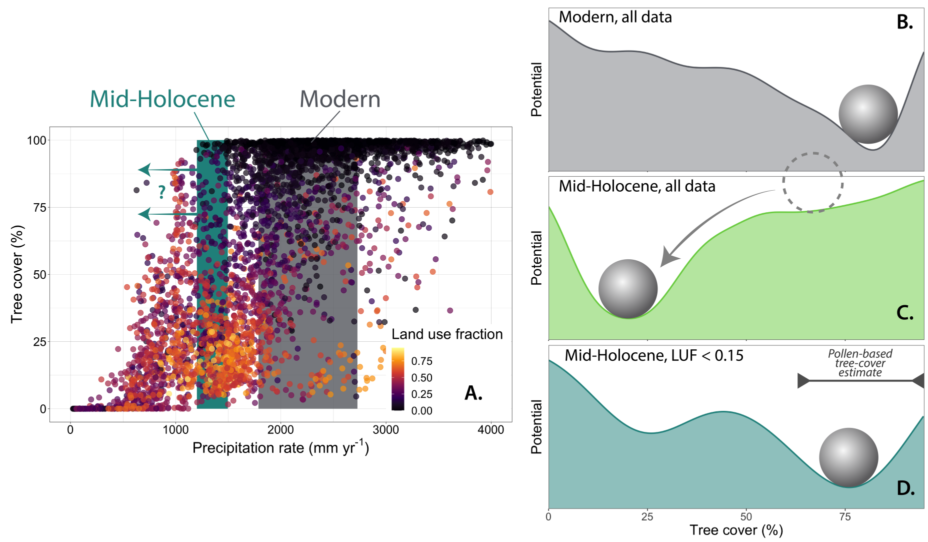

Figure 8: (**A**) Precipitation and tree cover in tropical South America (data from ref. [19]). Points colored by fraction of land use change in pixel. Isotope-derived modern precipitation rates for central Amazonia denoted by the gray rectangle. Mid-Holocene precipitation estimate shown in teal rectangle. (**B**) Potential diagram showing tree cover for the range of modern precipitation. Stable state is a high-tree cover forest. (**C**) Potential diagram for modern tree cover within the range of the mid-Holocene precipitation estimate. Within this range of precipitation, low tree cover savanna is the sole stable state. (**D**) Potential diagram for modern tree cover with mid-Holocene precipitation when only points with minimal land use fraction (LUF $< 15\%$ are shown, filtering out deforestation). Here, high tree cover forest remains a stable state of the system, consistent with proxy estimates of tree cover.

Fire is the only mechanism capable of driving bistability in our conceptual model and is required for bistability in some dynamic global vegetation model simulations [55]. But spatial data can appear bistable due to human-driven forcing that decreases tree cover independent from precipitation [19]. Bistability in a system is driven by feedbacks, not forcings, so if human-driven forcing (*i.e.* deforestation and anthropogenic fire) leads to apparent bistability we cannot characterize the system as bistable. Alternatively, it is possible that fire-aridity feedbacks are stronger today than in the mid-Holocene, characterizing the system as bistable and suggesting Amazon tree cover is less resilient to drying today regardless of human interference.

We test whether Amazon tree cover is as resilient to drying today as in the mid-Holocene by comparing our mid-Holocene reconstructions to modern data with and without accounting for land use (human-driven forcing). Figure 8A shows precipitation and tree cover across tropical South America today with data points colored by the land use fraction in each pixel (data from ref. [19]). Using these data, we can construct potential diagrams to identify the stable states of the system under different precipitation conditions. Potential diagrams are normalized, inverted PDFs (probability density function) of tree cover data for a given range of precipitation. The wells in a potential diagram reflect stable attractors, or stable states, and the ball represents the actual state of the system. For the modern precipitation range—defined by the RTM inversion of modern $\Delta\delta^{18}O$ data (Fig. 5)—the potential diagram shows a deep potential well at high tree cover, the stable state of the system (Fig. 8B).

Under mid-Holocene precipitation the high tree cover well shallows, tipping the ball to the new, low tree cover stable state (Fig. 8C). While this conflicts with evidence for high tree cover in the mid-Holocene [59, 138, 29, 21, 22], suggesting tree cover is less resilient to drying today, it is mostly an artifact of the intensification of modern human land use. When all pixels where the land use fraction exceeds 15% are removed, high tree cover forests remain the stable state for modern vegetation at low, mid-Holocene precipitation rates (Fig. 8E). This brings the modern precipitation-tree cover data in agreement with our mid-Holocene reconstructions, suggesting that in the absence of human disturbance, Amazon tree cover today is probably as resilient to drying as in the mid-Holocene.

6.4. Implications for the future of Amazon tree cover

Despite the vast uncertainty associated with model predictions and modern observations, some agreement surrounding the future of Amazon vegetation is emerging [20, 19]. Malhi et al., (2009) show that correcting for precipitation biases in models is crucial for predicting future vegetation assuming the modern spatial distribution of vegetation holds over time. When doing so, grasslands are an unlikely future state of Amazon vegetation [20]. More recently, Ahlström et al., (2017) demonstrate that additional corrections for land use, along with precipitation bias-corrections, bring models and observations into agreement that Amazon tree cover is resilient to drying. While our analysis cannot inform how biodiversity or vegetation species composition responds to drying, our results confirm that tree cover can remain high even when precipitation appears to fall well below future projections (*e.g.* Fig.

5). In the absence of human interference, our analysis could not identify feedbacks that invalidate this conclusion.

Drying alone, at least within the precipitation range studied here, does not pose a major threat to Amazon tree cover within our study region, but land use does. For example, impacts of modern human deforestation on Amazon water cycling are already measurable. Deforested watersheds show increased runoff, balancing the loss of evapotranspiration [97, 141, 142, 143, 144, 145]. While deforestation reduces tree cover without directly influencing precipitation (Fig. 1) the loss in moisture recycling may lead to a decrease in precipitation, especially in the western Amazon [58, 57]. Drying can also allow for more deforestation by increasing the effectiveness of methods that use fire [46, 45], setting the stage for a positive feedback between deforestation and aridity [47].

Temperature increases may also threaten Amazon vegetation. While we do not address the vegetation response to temperature (mid-Holocene temperatures were similar to pre-Industrial; Supplemental Fig. S10), some modeling work suggests the modern Amazon is near a "thermal threshold" where warming has a much larger effect on vegetation than cooling [146]. Future work reconstructing precipitation and vegetation in warmer and colder paleoclimate states will help account for the role of temperature in climate-vegetation relationships.

The geometry of savanna expansion and fire is another key difference that separates the mid-Holocene from modern forest loss. In the mid-Holocene most grassland expansion and fire was limited to forest-grassland interfaces [29, 21]. The core forested region of the Amazon Basin remained intact and not fragmented. By contrast, deforestation today extends far into the Amazon Basin, allowing human-driven activity to fragment forested regions and exert ecological stress from the inside-out. This is especially dangerous because human activity deep in the basin interior brings fires closer to core, annually inundated floodplain regions, which may be particularly vulnerable to forest loss and grassland expansion due to their low local tree cover and longer ecological recovery times [147]. Taken together, this suggests human activity can strengthen the fire feedback, perhaps making tree cover more sensitive to drying than it has been in the past.

7. Conclusion

We attribute the persistence of high central and western Amazon tree cover in the mid-Holocene to resilience to drying rather than to nominal aridification [21, 22]. Our results suggest Amazon tree cover is highly resilient to the magnitude of drying predicted in the worst-case-scenario, bias-corrected future climate projections (RCP8.5), although forest species composition may likely change. When human land use is locally, but not regionally intensive, mid-Holocene climate-vegetation patterns reveal that Amazon forests are not strongly sensitive to precipitation change (Fig. 4) and high tree cover persists likely because natural fires and the MRF were not strong enough feedbacks to drive widespread dieback. An important implication of this finding is, without human interference, feedbacks that amplify forest loss (particularly fire feedbacks) are too weak to tip Amazon forests to a grassland state, at least under mid-Holocene conditions. This resilience likely holds in seasonally dry conditions, inferred for the mid-Holocene, when fires are more common [44, 45], evergreen trees are water-stressed [36], and forests take longer to recover from drought [37].

The bulk of modern data indicate mid-Holocene levels of drying should yield a savanna-state, but accounting for land use brings observations, models [19], and paleoclimate reconstructions into agreement that Amazon tree cover is resilient to crossing below the 2,000 mm/yr precipitation threshold. We argue that, in the absence of extensive anthropogenic deforestation and fire, modern tree cover is just as resilient to drying as it was in the mid-Holocene. Even under the most drastic projections of future aridification, human-driven deforestation, not drying, will play the larger role in the evolution of Amazon tree cover.

Our proxy-model approach allows for a direct comparison between past and modern conditions and leaves room for future work to investigate other forms of resilience. For example, it is unclear how mid-Holocene biodiversity, ecosystem heterogeneity, and rainfall variability affected past resilience [14, 15, 16, 148]. Did these factors act to maintain Amazon forests despite growing water stress? Additionally, the Amazon's resilience to mid-Holocene drying fundamentally depends on our definition of the forest's function. We use tree cover as a proxy for the system's function because it is easier to compare past and present states. But ecosystem function may be defined by other characteristics like biodiversity or species composition and the resilience of these to mid-Holocene drying remains unknown. Future mid-Holocene paleoecological work will provide a more comprehensive perspective to the Amazon ecosystem resilience to drying.

We agree that ongoing anthropogenic fire and deforestation pose a serious threat to the survival of the rainforest [7, 10, 11]. Without human interference, feedbacks that can tip a forested system to a grassland may be too weak to do so in the range of future precipitation projections. But fire and deforestation leave a notable imprint in the Amazon Basin by extending far into the interior of forested regions and providing mechanisms to strengthen the feedbacks capable of causing widespread forest loss [47]. The resilience of Amazon vegetation to drying when human interference is minimal implies that, despite global climate change, curbing fire and deforestation will have the most immediate and long-lasting effect on the preservation of Amazon tree cover.

Data Availability

All proxy and DGVM data are available in the supplemental material of this manuscript. The following data can also be downloaded from their original sources. Charcoal data can be downloaded from the Global Charcoal Database (GCD version 2.0) using the paleofire package in R (`https://gpwg.paleofire.org/`). Pollen data can be downloaded from the Neotoma database (`https://www.neotomadb.org/`) and the ACER pollen and charcoal database (see supplement of ref. [117]). The Tigre Perdido isotope record [102] (part of the western composite site) can be downloaded from the SISAL database (siteID: 25). The Diamante record [32] (also part of the western composite) was provided by H. Cheng. The Paraíso record can be found in the supplement of ref. [30]. The time-interpolated and temperature-corrected $\delta^{18}O$ and $\Delta\delta^{18}O$ data are in the supplement of this text. The reactive transport model code can be found in the supplement of ref. [103] or at `https://github.com/tykukla/Vapor_Transport_Model_KuklaEtAl2019`.

Competing Interests Statement

The authors declare no competing interests.

ACKNOWLEDGMENTS

We thank C. Hoorn, R. B. Jackson, X. Wang, F. W. Cruz, A. Baresch, and J. K. C. Rugenstein for thoughtful discussion. We also thank H. Cheng for sharing speleothem data used in this study. We acknowledge the SISAL (Speleothem Isotopes Synthesis and Analysis) working group and data contributors. SISAL is a working group of the Past Global Changes (PAGES) programme. We acknowledge the World Climate Research Programme's Working Group on Coupled Modelling, which is responsible for CMIP, and we thank the climate modeling groups for producing and making available their model output. For CMIP the U.S. Department of Energy's Program for Climate Model Diagnosis and Intercomparison provides coordinating support and led development of software infrastructure in partnership with the Global Organization for Earth System Science Portals. We thank developers and providers of all data sources used in this study including GPCCv7 and PMIP3/CMIP5. T. K. acknowledges funding from a Stanford University McGee Grant and a Geological Society of America Student Research Grant. S. Y. M. acknowledges funding from the European Commission (Marie Curie Fellowship 792197).

References

[1] C. S. Holling, Resilience and Stability of Ecological Systems, Annual Review of Ecology and Systematics 4 (1973) 1–23. doi:10.1146/annurev.es.04.110173.000245.

[2] L. H. Gunderson, Ecological Resilience—In Theory and Application, Annual Review of Ecology and Systematics 31 (2000) 425–439. doi:10.1146/annurev.ecolsys.31.1.425.

[3] K. Kombiadou, S. Costas, A. R. Carrasco, T. A. Plomaritis, Ó. Ferreira, A. Matias, Bridging the gap between resilience and geomorphology of complex coastal systems, Earth-Science Reviews 198 (2019) 102934. doi:10.1016/j.earscirev.2019.102934.

[4] M. Scheffer, S. R. Carpenter, Catastrophic regime shifts in ecosystems: Linking theory to observation, Trends in Ecology & Evolution 18 (2003) 648–656. doi:10.1016/j.tree.2003.09.002.

[5] K. H. Cook, E. K. Vizy, Effects of Twenty-First-Century Climate Change on the Amazon Rain Forest, Journal of Climate 21 (2008) 542–560. doi:10.1175/2007JCLI1838.1.

[6] W. Li, R. Fu, R. E. Dickinson, Rainfall and its seasonality over the Amazon in the 21st century as assessed by the coupled models for the IPCC AR4, Journal of Geophysical Research 111 (2006). doi:10.1029/2005JD006355.

[7] I. Amigo, The Amazon's Fragile Future (When will the Amazon hit a Tipping Point?), Nature (Magazine article) (2020).

[8] C. A. Nobre, L. D. S. Borma, 'Tipping points' for the Amazon forest, Current Opinion in Environmental Sustainability 1 (2009) 28–36. doi:10.1016/j.cosust.2009.07.003.

[9] Y. Le Page, D. Morton, C. Hartin, B. Bond-Lamberty, J. M. C. Pereira, G. Hurtt, G. Asrar, Synergy between land use and climate change increases future fire risk in Amazon forests, Earth System Dynamics 8 (2017) 1237–1246. doi:10.5194/esd-8-1237-2017.

[10] T. E. Lovejoy, C. Nobre, Amazon Tipping Point, Science Advances 4 (2018) eaat2340. doi:10.1126/sciadv.aat2340.

[11] T. E. Lovejoy, C. Nobre, Amazon tipping point: Last chance for action, Science Advances 5 (2019) eaba2949. doi:10.1126/sciadv.aba2949.

[12] D. C. Nepstad, C. M. Stickler, B. S. Filho, F. Merry, Interactions among Amazon land use, forests and climate: Prospects for a near-term forest tipping point, Philosophical Transactions of the Royal Society B: Biological Sciences 363 (2008) 1737–1746. doi:10.1098/rstb.2007.0036.

[13] E. A. Davidson, A. C. de Araújo, P. Artaxo, J. K. Balch, I. F. Brown, M. M. C. Bustamante, M. T. Coe, R. S. DeFries, M. Keller, M. Longo, J. W. Munger, W. Schroeder, B. S. Soares-Filho, C. M. Souza, S. C. Wofsy, The Amazon basin in transition, Nature 481 (2012) 321–328. doi:10.1038/nature10717.

[14] N. M. Levine, K. Zhang, M. Longo, A. Baccini, O. L. Phillips, S. L. Lewis, E. Alvarez-Dávila, A. C. Segalin de Andrade, R. J. W. Brienen, T. L. Erwin, T. R. Feldpausch, A. L. Monteagudo Mendoza, P. Nuñez Vargas, A. Prieto, J. E. Silva-Espejo, Y. Malhi, P. R. Moorcroft, Ecosystem heterogeneity determines the ecological resilience of the Amazon to climate change, Proceedings of the National Academy of Sciences 113 (2016) 793–797. doi:10.1073/pnas.1511344112.

[15] B. Sakschewski, W. von Bloh, A. Boit, L. Poorter, M. Peña-Claros, J. Heinke, J. Joshi, K. Thonicke, Resilience of Amazon forests emerges from plant trait diversity, Nature Climate Change 6 (2016) 1032–1036. doi:10.1038/nclimate3109.

[16] E. H. van Nes, M. Scheffer, Implications of spatial heterogeneity for catastrophic regime shifts in ecosystems, Ecology 86 (2005) 1797–1807. doi:10.1890/04-0550.

[17] C. Ciemer, N. Boers, M. Hirota, J. Kurths, F. Müller-Hansen, R. S. Oliveira, R. Winkelmann, Higher resilience to climatic disturbances in tropical vegetation exposed to more variable rainfall, Nature Geoscience 12 (2019) 174–179. doi:10.1038/s41561-019-0312-z.

[18] M. Hirota, M. Holmgren, E. H. Van Nes, M. Scheffer, Global Resilience of Tropical Forest and Savanna to Critical Transitions, Science 334 (2011) 232–235. doi:10.1126/science.1210657.

[19] A. Ahlström, J. G. Canadell, G. Schurgers, M. Wu, J. A. Berry, K. Guan, R. B. Jackson, Hydrologic resilience and Amazon productivity, Nature Communications 8 (2017). doi:10.1038/s41467-017-00306-z.

[20] Y. Malhi, L. E. O. C. Aragao, D. Galbraith, C. Huntingford, R. Fisher, P. Zelazowski, S. Sitch, C. McSweeney, P. Meir, Exploring the likelihood and mechanism of a climate-change-induced dieback of the Amazon rainforest, Proceedings of the National Academy of Sciences 106 (2009) 20610–20615. doi:10.1073/pnas.0804619106.

[21] R. J. Smith, F. E. Mayle, Impact of mid- to late Holocene precipitation changes on vegetation across lowland tropical South America: A paleo-data synthesis, Quaternary Research 89 (2018) 134–155. doi:10.1017/qua.2017.89.

[22] M. N. Nascimento, G. S. Martins, R. C. Cordeiro, B. Turcq, L. S. Moreira, M. B. Bush, Vegetation response to climatic changes in western Amazonia over the last 7,600 years, Journal of Biogeography 46 (2019) 2389–2406. doi:10.1111/jbi.13704.

[23] P. A. Baker, C. A. Rigsby, G. O. Seltzer, S. C. Fritz, T. K. Lowenstein, N. P. Bacher, C. Veliz, Tropical climate changes at millennial and orbital timescales on the Bolivian Altiplano, Nature 409 (2001) 698–701. doi:10.1038/35055524.

[24] P. A. Baker, G. O. Seltzer, S. C. Fritz, R. B. Dunbar, M. J. Grove, P. M. Tapia, S. L. Cross, H. D. Rowe, J. P. Broda, The History of South American Tropical Precipitation for the Past 25,000 Years, Science 291 (2001) 640–643. doi:10.1126/science.291.5504.640.

[25] S. C. Fritz, P. A. Baker, G. O. Seltzer, A. Ballantyne, P. Tapia, H. Cheng, R. L. Edwards, Quaternary glaciation and hydrologic variation in the South American tropics as reconstructed from the Lake Titicaca drilling project, Quaternary Research 68 (2007) 410–420. doi:10.1016/j.yqres.2007.07.008.

[26] M. C. Campos, C. M. Chiessi, M. Prange, S. Mulitza, H. Kuhnert, A. Paul, I. M. Venancio, A. L. S. Albuquerque, F. W. Cruz, A. Bahr, A new mechanism for millennial scale positive precipitation anomalies

over tropical South America, Quaternary Science Reviews 225 (2019) 105990. doi:10.1016/j.quascirev.2019.105990.

[27] T. E. Nace, P. A. Baker, G. S. Dwyer, C. G. Silva, C. A. Rigsby, S. J. Burns, L. Giosan, B. Otto-Bliesner, Z. Liu, J. Zhu, The role of North Brazil Current transport in the paleoclimate of the Brazilian Nordeste margin and paleoceanography of the western tropical Atlantic during the late Quaternary, Palaeogeography, Palaeoclimatology, Palaeoecology 415 (2014) 3–13. doi:10.1016/j.palaeo.2014.05.030.

[28] S. Mulitza, C. M. Chiessi, E. Schefuß, J. Lippold, D. Wichmann, B. Antz, A. Mackensen, A. Paul, M. Prange, K. Rehfeld, M. Werner, T. Bickert, N. Frank, H. Kuhnert, J. Lynch-Stieglitz, R. C. Portilho-Ramos, A. O. Sawakuchi, M. Schulz, T. Schwenk, R. Tiedemann, M. Vahlenkamp, Y. Zhang, Synchronous and proportional deglacial changes in Atlantic meridional overturning and northeast Brazilian precipitation: AMOC and Precipitation over NE Brazil, Paleoceanography 32 (2017) 622–633. doi:10.1002/2017PA003084.

[29] F. E. Mayle, M. J. Power, Impact of a drier Early–Mid-Holocene climate upon Amazonian forests, Philosophical Transactions of the Royal Society B: Biological Sciences 363 (2008) 1829–1838. doi:10.1098/rstb.2007.0019.

[30] X. Wang, R. L. Edwards, A. S. Auler, H. Cheng, X. Kong, Y. Wang, F. W. Cruz, J. A. Dorale, H.-W. Chiang, Hydroclimate changes across the Amazon lowlands over the past 45,000 years, Nature 541 (2017) 204–207. doi:10.1038/nature20787.

[31] F. W. Cruz, M. Vuille, S. J. Burns, X. Wang, H. Cheng, M. Werner, R. L. Edwards, I. Karmann, A. S. Auler, H. Nguyen, Orbitally driven east–west antiphasing of South American precipitation, Nature Geoscience 2 (2009) 210–214. doi:10.1038/ngeo444.

[32] H. Cheng, A. Sinha, F. W. Cruz, X. Wang, R. L. Edwards, F. M. D'Horta, C. C. Ribas, M. Vuille, L. D. Stott, A. S. Auler, Climate change patterns in Amazonia and biodiversity, Nature Communications 4 (2013) 1–6. doi:10.1038/ncomms2415.

[33] A. C. Staver, S. Archibald, S. A. Levin, The Global Extent and Determinants of Savanna and Forest as Alternative Biome States, Science 334 (2011) 230–232.

[34] T. M. Lenton, H. Held, E. Kriegler, J. W. Hall, W. Lucht, S. Rahmstorf, H. J. Schellnhuber, Tipping elements in the Earth's climate system, Proceedings of the National Academy of Sciences 105 (2008) 1786–1793. doi:10.1073/pnas.0705414105.

[35] D. C. Zemp, C.-F. Schleussner, H. M. J. Barbosa, M. Hirota, V. Montade, G. Sampaio, A. Staal, L. Wang-Erlandsson, A. Rammig, Self-amplified Amazon forest loss due to vegetation-atmosphere feedbacks, Nature Communications 8 (2017). doi:10.1038/ncomms14681.

[36] K. Guan, M. Pan, H. Li, A. Wolf, J. Wu, D. Medvigy, K. K. Caylor, J. Sheffield, E. F. Wood, Y. Malhi, M. Liang, J. S. Kimball, S. R. Saleska, J. Berry, J. Joiner, A. I. Lyapustin, Photosynthetic seasonality of global tropical forests constrained by hydroclimate, Nature Geoscience 8 (2015) 284–289. doi:10.1038/ngeo2382.

[37] J. Verbesselt, N. Umlauf, M. Hirota, M. Holmgren, E. H. Van Nes, M. Herold, A. Zeileis, M. Scheffer, Remotely sensed resilience of tropical forests, Nature Climate Change 6 (2016) 1028–1031. doi:10.1038/nclimate3108.

[38] B. J. Enquist, C. A. F. Enquist, Long-term change within a Neotropical forest: Assessing differential functional and floristic responses to disturbance and drought: DIFFERENTIAL FUNCTIONAL RESPONSES TO CLIMATE CHANGE IN A TROPICAL FOREST, Global Change Biology 17 (2011) 1408–1424. doi:10.1111/j.1365-2486.2010.02326.x.

[39] A. T. Leite-Filho, V. Y. Sousa Pontes, M. H. Costa, Effects of Deforestation on the Onset of the Rainy Season and the Duration of Dry Spells in Southern Amazonia, Journal of Geophysical Research: Atmospheres 124 (2019) 5268–5281. doi:10.1029/2018JD029537.

[40] A. T. Leite-Filho, M. H. Costa, R. Fu, The southern Amazon rainy season: The role of deforestation and its interactions with

large-scale mechanisms, International Journal of Climatology (2019). doi:10.1002/joc.6335.

[41] W. Li, R. Fu, Transition of the Large-Scale Atmospheric and Land Surface Conditions from the Dry to the Wet Season over Amazonia as Diagnosed by the ECMWF Re-Analysis, Journal of Climate 17 (2004) 2637–2651. doi:10.1175/1520-0442(2004)017<2637:TOTLAA>2.0.CO;2.

[42] A. Kleidon, M. Heimann, Assessing the role of deep rooted vegetation in the climate system with model simulations: Mechanism, comparison to observations and implications for Amazonian deforestation, Climate Dynamics 16 (2000) 183–199. doi:10.1007/s003820050012.

[43] J. S. Wright, R. Fu, J. R. Worden, S. Chakraborty, N. E. Clinton, C. Risi, Y. Sun, L. Yin, Rainforest-initiated wet season onset over the southern Amazon, Proceedings of the National Academy of Sciences 114 (2017) 8481–8486. doi:10.1073/pnas.1621516114.

[44] D. Ray, D. Nepstad, P. Moutinho, Micrometeorological and canopy controls of fire susceptibility in a forested Amazon landscape, Ecological Applications 15 (2005) 1664–1678. doi:10.1890/05-0404.

[45] L. E. O. Aragão, Y. Malhi, N. Barbier, A. Lima, Y. Shimabukuro, L. Anderson, S. Saatchi, Interactions between rainfall, deforestation and fires during recent years in the Brazilian Amazonia, Philosophical Transactions of the Royal Society B: Biological Sciences 363 (2008) 1779–1785. doi:10.1098/rstb.2007.0026.

[46] J. Barlow, E. Berenguer, R. Carmenta, F. França, Clarifying Amazonia's burning crisis, Global Change Biology 26 (2020) 319–321. doi:10.1111/gcb.14872.

[47] A. Staal, B. M. Flores, A. P. D. Aguiar, J. H. C. Bosmans, I. Fetzer, O. A. Tuinenburg, Feedback between drought and deforestation in the Amazon, Environmental Research Letters 15 (2020) 044024. doi:10.1088/1748-9326/ab738e.

[48] W. J. Bond, What Limits Trees in C$_4$ Grasslands and Savannas?, Annual Review of Ecology, Evolution, and Systematics 39 (2008) 641–659. doi:10.1146/annurev.ecolsys.39.110707.173411.

[49] W. J. Bond, F. I. Woodward, G. F. Midgley, The global distribution of ecosystems in a world without fire, New Phytologist 165 (2005) 525–538. doi:10.1111/j.1469-8137.2004.01252.x.

[50] F. Mouillot, C. B. Field, Fire history and the global carbon budget: A 1ox 1o fire history reconstruction for the 20th century, Global Change Biology 11 (2005) 398–420. doi:10.1111/j.1365-2486.2005.00920.x.

[51] M. A. Cochrane, K. C. Ryan, Fire and Fire ecology: Concepts and principles, in: Tropical Fire Ecology, Springer, Berlin, Heidelberg, 2009, pp. 25–62.

[52] R. A. Betts, P. M. Cox, M. Collins, P. P. Harris, C. Huntingford, C. D. Jones, The role of ecosystem-atmosphere interactions in simulated Amazonian precipitation decrease and forest dieback under global climate warming, Theoretical and Applied Climatology 78 (2004). doi:10.1007/s00704-004-0050-y.

[53] P. M. Cox, R. A. Betts, C. D. Jones, S. A. Spall, I. J. Totterdell, Acceleration of global warming due to carbon-cycle feedbacks in a coupled climate model, Nature 408 (2000) 184–187.

[54] P. M. Cox, R. A. Betts, M. Collins, P. P. Harris, C. Huntingford, C. D. Jones, Amazonian forest dieback under climate-carbon cycle projections for the 21st century, Theoretical and Applied Climatology 78 (2004). doi:10.1007/s00704-004-0049-4.

[55] G. Lasslop, V. Brovkin, C. H. Reick, S. Bathiany, S. Kloster, Multiple stable states of tree cover in a global land surface model due to a fire-vegetation feedback: MULTISTABILITY OF TREE COVER, Geophysical Research Letters 43 (2016) 6324–6331. doi:10.1002/2016GL069365.

[56] A. Staal, S. C. Dekker, M. Hirota, E. H. van Nes, Synergistic effects of drought and deforestation on the resilience of the southeastern Amazon rainforest, Ecological Complexity 22 (2015) 65–75. doi:10.1016/j.ecocom.2015.01.003.

[57] D. C. Zemp, C.-F. Schleussner, H. M. J. Barbosa, R. J. van der Ent, J. F. Donges, J. Heinke, G. Sampaio, A. Rammig, On the importance

of cascading moisture recycling in South America, Atmospheric Chemistry and Physics 14 (2014) 13337–13359. doi:10.5194/acp-14-13337-2014.

[58] A. Staal, O. A. Tuinenburg, J. H. C. Bosmans, M. Holmgren, E. H. van Nes, M. Scheffer, D. C. Zemp, S. C. Dekker, Forest-rainfall cascades buffer against drought across the Amazon, Nature Climate Change 8 (2018) 539–543. doi:10.1038/s41558-018-0177-y.

[59] S. G. Haberle, M. A. Maslin, Late Quaternary Vegetation and Climate Change in the Amazon Basin Based on a 50,000 Year Pollen Record from the Amazon Fan, ODP Site 932, Quaternary Research 51 (1999) 27–38. doi:10.1006/qres.1998.2020.

[60] B. Smith, D. Wårlind, A. Arneth, T. Hickler, P. Leadley, J. Siltberg, S. Zaehle, Implications of incorporating N cycling and N limitations on primary production in an individual-based dynamic vegetation model, Biogeosciences 11 (2014) 2027–2054. doi:10.5194/bg-11-2027-2014.

[61] S. I. Higgins, W. J. Bond, E. C. February, A. Bronn, D. I. W. Euston-Brown, B. Enslin, N. Govender, L. Rademan, S. O'Regan, A. L. F. Potgieter, S. Scheiter, R. Sowry, L. Trollope, W. S. W. Trollope, Effects of four decades of fire manipulation on woody vegetation structure in savanna, Ecology 88 (2007) 1119–1125.

[62] W. Bond, G. Midgley, F. Woodward, What controls South African vegetation — climate or fire?, South African Journal of Botany 69 (2003) 79–91. doi:10.1016/S0254-6299(15)30362-8.

[63] C. G. Trapnell, Ecological Results of Woodland and Burning Experiments in Northern Rhodisia, The Journal of Ecology 47 (1959) 129. doi:10.2307/2257252.

[64] D. Louppe, N. Oattara, A. C. Líbaly, The effects of brush fires on vegetation: The Aubréville fire plots after 60 years, Commonwealth Forestry Review 74 (1995) 288–292.

[65] J. C. Z. Woinarski, J. Risler, L. Kean, Response of vegetation and vertebrate fauna to 23 years of fire exclusion in a tropical Eucalyptus open forest, Northern Territory, Australia: IMPACTS OF LONG-

TERM FIRE EXCLUSION, Austral Ecology 29 (2004) 156–176. doi:10.1111/j.1442-9993.2004.01333.x.

[66] D. W. Peterson, P. B. Reich, PRESCRIBED FIRE IN OAK SAVANNA: FIRE FREQUENCY EFFECTS ON STAND STRUCTURE AND DYNAMICS, Ecological Applications 11 (2001) 914–927. doi:10.1890/1051-0761(2001)011[0914:PFIOSF]2.0.CO;2.

[67] W. J. Bond, G. F. Midgley, F. I. Woodward, The importance of low atmospheric CO2 and fire in promoting the spread of grasslands and savannas, Global Change Biology 9 (2003) 973–982. doi:10.1046/j.1365-2486.2003.00577.x.

[68] S. C. Fritz, P. A. Baker, T. K. Lowenstein, G. O. Seltzer, C. A. Rigsby, G. S. Dwyer, P. M. Tapia, K. K. Arnold, T.-L. Ku, S. Luo, Hydrologic variation during the last 170,000 years in the southern hemisphere tropics of South America, Quaternary Research 61 (2004) 95–104. doi:10.1016/j.yqres.2003.08.007.

[69] H. A. de Freitas, L. C. R. Pessenda, R. Aravena, S. E. M. Gouveia, A. de Souza Ribeiro, R. Boulet, Late Quaternary Vegetation Dynamics in the Southern Amazon Basin Inferred from Carbon Isotopes in Soil Organic Matter, Quaternary Research 55 (2001) 39–46. doi:10.1006/qres.2000.2192.

[70] L. S. Reis, J. T. F. Guimarães, P. W. M. Souza-Filho, P. K. Sahoo, M. M. J. C. de Figueiredo, E. B. de Souza, T. C. Giannini, Environmental and vegetation changes in southeastern Amazonia during the late Pleistocene and Holocene, Quaternary International 449 (2017) 83–105. doi:10.1016/j.quaint.2017.04.031.

[71] M. Abbott, Holocene hydrological reconstructions from stable isotopes and paleolimnology, Cordillera Real, Bolivia, Quaternary Science Reviews 19 (2000) 1801–1820. doi:10.1016/S0277-3791(00)00078-0.

[72] M. B. Abbott, B. B. Wolfe, A. P. Wolfe, G. O. Seltzer, R. Aravena, B. G. Mark, P. J. Polissar, D. T. Rodbell, H. D. Rowe, M. Vuille, Holocene paleohydrology and glacial history of the central Andes using multiproxy lake sediment studies, Palaeogeography, Palaeoclimatology, Palaeoecology 194 (2003) 123–138. doi:10.1016/S0031-0182(03)00274-8.

[73] A. Zular, A. O. Sawakuchi, C. M. Chiessi, F. M. d'Horta, F. W. Cruz, J. A. M. Demattê, C. C. Ribas, G. A. Hartmann, P. C. F. Giannini, E. A. A. Soares, The role of abrupt climate change in the formation of an open vegetation enclave in northern Amazonia during the late Quaternary, Global and Planetary Change 172 (2019) 140–149. doi:10.1016/j.gloplacha.2018.09.006.

[74] H. W. Arz, J. Pätzold, G. Wefer, Correlated Millennial-Scale Changes in Surface Hydrography and Terrigenous Sediment Yield Inferred from Last-Glacial Marine Deposits off Northeastern Brazil, Quaternary Research 50 (1998) 157–166.

[75] H. Behling, H. W. Arz, J. Pätzold, G. Wefer, Late Quaternary vegetational and climate dynamics in southeastern Brazil, inferences from marine cores GeoB 3229-2 and GeoB 3202-1, Palaeogeography, Palaeoclimatology, Palaeoecology 179 (2002) 227–243. doi:10.1016/S0031-0182(01)00435-7.

[76] P. M. Tapia, S. C. Fritz, P. A. Baker, G. O. Seltzer, R. B. Dunbar, A Late Quaternary diatom record of tropical climatic history from Lake Titicaca (Peru and Bolivia), Palaeogeography, Palaeoclimatology, Palaeoecology 194 (2003) 139–164. doi:10.1016/S0031-0182(03)00275-X.

[77] M. R. Morales, S. Bustos, B. I. Oxman, M. Pirola, P. Tchilinguirian, M. J. Orgeira, H. D. Yacobaccio, Exploring habitat diversity of mid-holocene hunter-gatherers in the South-Central Andes: Multiproxy analysis of Cruces Core 1 (TC1), Dry Puna of Jujuy, Argentina, Journal of Archaeological Science: Reports 18 (2018) 708–721. doi:10.1016/j.jasrep.2017.07.010.

[78] L. C. Pessenda, R. Boulet, R. Aravena, V. Rosolen, S. E. Gouveia, A. S. Ribeiro, M. Lamotte, Origin and dynamics of soil organic matter and vegetation changes during the Holocene in a forest-savanna transition zone, Brazilian Amazon region, The Holocene 11 (2001) 250–254. doi:10.1191/095968301668898509.

[79] M. Bush, A. Correa-Metrio, C. McMichael, S. Sully, C. Shadik, B. Valencia, T. Guilderson, M. Steinitz-Kannan, J. Overpeck, A 6900-year history of landscape modification by humans in lowland Ama-

zonia, Quaternary Science Reviews 141 (2016) 52–64. doi:10.1016/j.quascirev.2016.03.022.

[80] J. Watling, J. Iriarte, F. E. Mayle, D. Schaan, L. C. R. Pessenda, N. J. Loader, F. A. Street-Perrott, R. E. Dickau, A. Damasceno, A. Ranzi, Impact of pre-Columbian "geoglyph" builders on Amazonian forests, Proceedings of the National Academy of Sciences 114 (2017) 1868–1873. doi:10.1073/pnas.1614359114.

[81] J. F. Carson, B. S. Whitney, F. E. Mayle, J. Iriarte, H. Prumers, J. D. Soto, J. Watling, Environmental impact of geometric earthwork construction in pre-Columbian Amazonia, Proceedings of the National Academy of Sciences 111 (2014) 10497–10502. doi:10.1073/pnas.1321770111.

[82] J. Watling, M. P. Shock, G. Z. Mongeló, F. O. Almeida, T. Kater, P. E. De Oliveira, E. G. Neves, Direct archaeological evidence for Southwestern Amazonia as an early plant domestication and food production centre, PLOS ONE 13 (2018) e0199868. doi:10.1371/journal.pone.0199868.

[83] T. D. Dillehay, J. Rossen, T. C. Andres, D. E. Williams, Preceramic Adoption of Peanut, Squash, and Cotton in Northern Peru, Science 316 (2007) 1890–1893. doi:10.1126/science.1141395.

[84] P. Riris, M. Arroyo-Kalin, Widespread population decline in South America correlates with mid-Holocene climate change, Scientific Reports 9 (2019). doi:10.1038/s41598-019-43086-w.

[85] J. Iriarte, S. Elliot, S. Y. Maezumi, D. Alves, R. Gonda, M. Robinson, J. G. De Souza, J. Watling, J. Handley, The origins of Amazonian landscapes: Plant cultivation, domestication and the spread of food production in tropical South America, Quaternary Science Reviews Accepted (2020).

[86] S. Y. Maezumi, B. S. Whitney, F. E. Mayle, J. Gregorio de Souza, J. Iriarte, Reassessing climate and pre-Columbian drivers of paleofire activity in the Bolivian Amazon, Quaternary International 488 (2018) 81–94. doi:10.1016/j.quaint.2017.11.053.

[87] L. Martin, J. Bertaux, T. Corrège, M.-P. Ledru, P. Mourguiart, A. Sifeddine, F. Soubiès, D. Wirrmann, K. Suguio, B. Turcq, Astronomical Forcing of Contrasting Rainfall Changes in Tropical South America between 12,400 and 8800 cal yr B.P., Quaternary Research 47 (1997) 117–122. doi:10.1006/qres.1996.1866.

[88] P. A. Baker, S. C. Fritz, Nature and causes of Quaternary climate variation of tropical South America, Quaternary Science Reviews 124 (2015) 31–47. doi:10.1016/j.quascirev.2015.06.011.

[89] C. C. Mason, B. W. Romans, D. F. Stockli, R. W. Mapes, A. Fildani, Detrital zircons reveal sea-level and hydroclimate controls on Amazon River to deep-sea fan sediment transfer, Geology 47 (2019) 563–567. doi:10.1130/G45852.1.

[90] W. Abouchami, M. Zabel, Climate forcing of the Pb isotope record of terrigenous input into the Equatorial Atlantic, Earth and Planetary Science Letters 213 (2003) 221–234. doi:10.1016/S0012-821X(03)00304-2.

[91] X. Liu, D. S. Battisti, The Influence of Orbital Forcing of Tropical Insolation on the Climate and Isotopic Composition of Precipitation in South America, Journal of Climate 28 (2015) 4841–4862. doi:10.1175/JCLI-D-14-00639.1.

[92] M. H. Shimizu, G. Sampaio, I. M. Venancio, J. Maksic, Seasonal changes of the South American monsoon system during the Mid-Holocene in the CMIP5 simulations, Climate Dynamics (2020). doi:10.1007/s00382-020-05137-1.

[93] J. Zhou, K.-M. Lau, Does a Monsoon Climate Exist over South America?, Journal of Climate 11 (1998) 1020–1040. doi:10.1175/1520-0442(1998)011<1020:DAMCEO>2.0.CO;2.

[94] V. B. S. Silva, V. E. Kousky, The South American Monsoon System: Climatology and Variability, in: S.-Y. S. Wang (Ed.), Modern Climatology, InTech, 2012. doi:10.5772/38565.

[95] E. A. B. Eltahir, R. L. Bras, Precipitation recycling in the Amazon basin, Quarterly Journal of the Royal Meteorological Society 120 (1994) 861–880. doi:10.1002/qj.49712051806.

[96] Z. Yang, F. Dominguez, Investigating Land Surface Effects on the Moisture Transport over South America with a Moisture Tagging Model, Journal of Climate 32 (2019) 6627–6644. doi:10.1175/JCLI-D-18-0700.1.

[97] M. C. Levy, A. V. Lopes, A. Cohn, L. G. Larsen, S. E. Thompson, Land Use Change Increases Streamflow Across the Arc of Deforestation in Brazil, Geophysical Research Letters 45 (2018) 3520–3530. doi:10.1002/2017GL076526.

[98] N. Zeng, R. E. Dickinson, X. Zeng, Climatic impact of Amazon deforestation–A mechanistic model study, Journal of Climate 9 (1996) 859–883.

[99] F. W. Cruz, S. J. Burns, M. Jercinovic, I. Karmann, W. D. Sharp, M. Vuille, Evidence of rainfall variations in Southern Brazil from trace element ratios (Mg/Ca and Sr/Ca) in a Late Pleistocene stalagmite, Geochimica et Cosmochimica Acta 71 (2007) 2250–2263. doi:10.1016/j.gca.2007.02.005.

[100] N. M. Strikis, F. W. Cruz, H. Cheng, I. Karmann, R. L. Edwards, M. Vuille, X. Wang, M. S. de Paula, V. F. Novello, A. S. Auler, Abrupt variations in South American monsoon rainfall during the Holocene based on a speleothem record from central-eastern Brazil, Geology 39 (2011) 1075–1078. doi:10.1130/G32098.1.

[101] V. F. Novello, F. W. Cruz, M. Vuille, N. M. Stríkis, R. L. Edwards, H. Cheng, S. Emerick, M. S. de Paula, X. Li, E. d. S. Barreto, I. Karmann, R. V. Santos, A high-resolution history of the South American Monsoon from Last Glacial Maximum to the Holocene, Scientific Reports 7 (2017). doi:10.1038/srep44267.

[102] M. van Breukelen, H. Vonhof, J. Hellstrom, W. Wester, D. Kroon, Fossil dripwater in stalagmites reveals Holocene temperature and rainfall variation in Amazonia, Earth and Planetary Science Letters 275 (2008) 54–60. doi:10.1016/j.epsl.2008.07.060.

[103] T. Kukla, M. J. Winnick, K. Maher, D. E. Ibarra, C. P. Chamberlain, The Sensitivity of Terrestrial $\underline{\delta}$ ^{18} O Gradients to Hydroclimate

Evolution, Journal of Geophysical Research: Atmospheres 124 (2019) 563–582. doi:10.1029/2018JD029571.

[104] M. J. Winnick, C. P. Chamberlain, J. K. Caves, J. M. Welker, Quantifying the isotopic 'continental effect', Earth and Planetary Science Letters 406 (2014) 123–133. doi:10.1016/j.epsl.2014.09.005.

[105] M. B. Hendricks, D. J. DePaolo, R. C. Cohen, Space and time variation of d18O and dD in precipitation: Can paleotemperature be estimated from ice cores?, Global Biogeochemical Cycles 14 (2000) 851–861.

[106] C. P. Chamberlain, M. J. Winnick, H. T. Mix, S. D. Chamberlain, K. Maher, The impact of neogene grassland expansion and aridification on the isotopic composition of continental precipitation, Global Biogeochemical Cycles 28 (2014) 992–1004. doi:10.1002/2014GB004822.

[107] A. Ampuero, N. M. Stríkis, J. Apaéstegui, M. Vuille, V. F. Novello, J. C. Espinoza, F. W. Cruz, H. Vonhof, V. C. Mayta, V. T. S. Martins, R. C. Cordeiro, V. Azevedo, A. Sifeddine, The Forest Effects on the Isotopic Composition of Rainfall in the Northwestern Amazon Basin, Journal of Geophysical Research: Atmospheres 125 (2020). doi:10.1029/2019JD031445.

[108] E. Salati, A. Dall'Olio, E. Matsui, J. R. Gat, Recycling of water in the Amazon Basin: An isotopic study, Water Resources Research 15 (1979) 1250–1258. doi:10.1029/WR015i005p01250.

[109] C. Hu, G. M. Henderson, J. Huang, S. Xie, Y. Sun, K. R. Johnson, Quantification of Holocene Asian monsoon rainfall from spatially separated cave records, Earth and Planetary Science Letters 266 (2008) 221–232. doi:10.1016/j.epsl.2007.10.015.

[110] J. K. Caves, M. J. Winnick, S. A. Graham, D. J. Sjostrom, A. Mulch, C. P. Chamberlain, Role of the westerlies in Central Asia climate over the Cenozoic, Earth and Planetary Science Letters 428 (2015) 33–43. doi:10.1016/j.epsl.2015.07.023.

[111] W. Dansgaard, Stable isotopes in precipitation, Tellus 16 (1964) 436–468. doi:10.3402/tellusa.v16i4.8993.

[112] A. Bailey, E. Posmentier, X. Feng, Patterns of evaporation and precipitation drive global isotopic changes in atmospheric moisture, Geophysical Research Letters 45 (2018) 7093–7101. doi:10.1029/2018GL078254.

[113] M. Moore, Z. Kuang, P. N. Blossey, A moisture budget perspective of the amount effect, Geophysical Research Letters 41 (2014) 1329–1335. doi:10.1002/2013GL058302.

[114] J.-E. Lee, I. Fung, D. J. DePaolo, C. C. Henning, Analysis of the global distribution of water isotopes using the NCAR atmospheric general circulation model, Journal of Geophysical Research 112 (2007) D16306. doi:10.1029/2006JD007657.

[115] J.-E. Lee, K. Johnson, I. Fung, Precipitation over South America during the Last Glacial Maximum: An analysis of the "amount effect" with a water isotope-enabled general circulation model, Geophysical Research Letters 36 (2009) L19701. doi:10.1029/2009GL039265.

[116] J. W. Williams, E. C. Grimm, J. L. Blois, D. F. Charles, E. B. Davis, S. J. Goring, R. W. Graham, A. J. Smith, M. Anderson, J. Arroyo-Cabrales, A. C. Ashworth, J. L. Betancourt, B. W. Bills, R. K. Booth, P. I. Buckland, B. B. Curry, T. Giesecke, S. T. Jackson, C. Latorre, J. Nichols, T. Purdum, R. E. Roth, M. Stryker, H. Takahara, The Neotoma Paleoecology Database, a multiproxy, international, community-curated data resource, Quaternary Research 89 (2018) 156–177. doi:10.1017/qua.2017.105.

[117] M. F. Sánchez Goñi, S. Desprat, A.-L. Daniau, F. C. Bassinot, J. M. Polanco-Martínez, S. P. Harrison, J. R. M. Allen, R. S. Anderson, H. Behling, R. Bonnefille, F. Burjachs, J. S. Carrión, R. Cheddadi, J. S. Clark, N. Combourieu-Nebout, C. J. C. Mustaphi, G. H. Debusk, L. M. Dupont, J. M. Finch, W. J. Fletcher, M. Giardini, C. González, W. D. Gosling, L. D. Grigg, E. C. Grimm, R. Hayashi, K. Helmens, L. E. Heusser, T. Hill, G. Hope, B. Huntley, Y. Igarashi, T. Irino, B. Jacobs, G. Jiménez-Moreno, S. Kawai, A. P. Kershaw, F. Kumon, I. T. Lawson, M.-P. Ledru, A.-M. Lézine, P. M. Liew, D. Magri, R. Marchant, V. Margari, F. E. Mayle, G. M. McKenzie, P. Moss, S. Müller, U. C. Müller, F. Naughton, R. M. Newnham, T. Oba, R. Pérez-Obiol, R. Pini, C. Ravazzi, K. H. Roucoux, S. M. Rucina,

L. Scott, H. Takahara, P. C. Tzedakis, D. H. Urrego, B. van Geel, B. G. Valencia, M. J. Vandergoes, A. Vincens, C. L. Whitlock, D. A. Willard, M. Yamamoto, The ACER pollen and charcoal database: A global resource to document vegetation and fire response to abrupt climate changes during the last glacial period, Earth System Science Data 9 (2017) 679–695. doi:10.5194/essd-9-679-2017.

[118] O. Blarquez, B. Vannière, J. R. Marlon, A.-L. Daniau, M. J. Power, S. Brewer, P. J. Bartlein, Paleofire: An R package to analyse sedimentary charcoal records from the Global Charcoal Database to reconstruct past biomass burning, Computers & Geosciences 72 (2014) 255–261. doi:10.1016/j.cageo.2014.07.020.

[119] J. R. Marlon, P. J. Bartlein, C. Carcaillet, D. G. Gavin, S. P. Harrison, P. E. Higuera, F. Joos, M. J. Power, I. C. Prentice, Climate and human influences on global biomass burning over the past two millennia, Nature Geoscience 1 (2008) 697–702. doi:10.1038/ngeo313.

[120] M. J. Power, J. Marlon, N. Ortiz, P. J. Bartlein, S. P. Harrison, F. E. Mayle, A. Ballouche, R. H. W. Bradshaw, C. Carcaillet, C. Cordova, S. Mooney, P. I. Moreno, I. C. Prentice, K. Thonicke, W. Tinner, C. Whitlock, Y. Zhang, Y. Zhao, A. A. Ali, R. S. Anderson, R. Beer, H. Behling, C. Briles, K. J. Brown, A. Brunelle, M. Bush, P. Camill, G. Q. Chu, J. Clark, D. Colombaroli, S. Connor, A.-L. Daniau, M. Daniels, J. Dodson, E. Doughty, M. E. Edwards, W. Finsinger, D. Foster, J. Frechette, M.-J. Gaillard, D. G. Gavin, E. Gobet, S. Haberle, D. J. Hallett, P. Higuera, G. Hope, S. Horn, J. Inoue, P. Kaltenrieder, L. Kennedy, Z. C. Kong, C. Larsen, C. J. Long, J. Lynch, E. A. Lynch, M. McGlone, S. Meeks, S. Mensing, G. Meyer, T. Minckley, J. Mohr, D. M. Nelson, J. New, R. Newnham, R. Noti, W. Oswald, J. Pierce, P. J. H. Richard, C. Rowe, M. F. Sanchez Goñi, B. N. Shuman, H. Takahara, J. Toney, C. Turney, D. H. Urrego-Sanchez, C. Umbanhowar, M. Vandergoes, B. Vanniere, E. Vescovi, M. Walsh, X. Wang, N. Williams, J. Wilmshurst, J. H. Zhang, Changes in fire regimes since the Last Glacial Maximum: An assessment based on a global synthesis and analysis of charcoal data, Climate Dynamics 30 (2008) 887–907. doi:10.1007/s00382-007-0334-x.

[121] B. Smith, I. C. Prentice, Representation of Vegetation Dynamics in

the Modelling of Terrestrial Ecosystems: Comparing Two Contrasting Approaches within European Climate Space, Global Ecology (2001) 18.

[122] A. Ahlström, P. A. Miller, B. Smith, Too early to infer a global NPP decline since 2000: TOO EARLY TO INFER A GLOBAL NPP DECLINE, Geophysical Research Letters 39 (2012). doi:10.1029/2012GL052336.

[123] K. Thonicke, S. Venevsky, S. Sitch, W. Cramer, The role of fire disturbance for global vegetation dynamics: Coupling fire into a Dynamic Global Vegetation Model: Fire disturbance and global vegetation dynamics, Global Ecology and Biogeography 10 (2001) 661–677. doi:10.1046/j.1466-822X.2001.00175.x.

[124] W. Hazeleger, C. Severijns, T. Semmler, S. Ştefănescu, S. Yang, X. Wang, K. Wyser, E. Dutra, J. M. Baldasano, R. Bintanja, P. Bougeault, R. Caballero, A. M. L. Ekman, J. H. Christensen, B. van den Hurk, P. Jimenez, C. Jones, P. Kållberg, T. Koenigk, R. McGrath, P. Miranda, T. van Noije, T. Palmer, J. A. Parodi, T. Schmith, F. Selten, T. Storelvmo, A. Sterl, H. Tapamo, M. Vancoppenolle, P. Viterbo, U. Willén, EC-Earth: A Seamless Earth-System Prediction Approach in Action, Bulletin of the American Meteorological Society 91 (2010) 1357–1364. doi:10.1175/2010BAMS2877.1.

[125] F. S. Pausata, G. Messori, Q. Zhang, Impacts of dust reduction on the northward expansion of the African monsoon during the Green Sahara period, Earth and Planetary Science Letters 434 (2016) 298–307. doi:10.1016/j.epsl.2015.11.049.

[126] Z. Lu, P. A. Miller, Q. Zhang, Q. Zhang, D. Wårlind, L. Nieradzik, J. Sjolte, B. Smith, Dynamic Vegetation Simulations of the Mid-Holocene Green Sahara, Geophysical Research Letters 45 (2018) 8294–8303. doi:10.1029/2018GL079195.

[127] M. C. Hansen, P. V. Potapov, R. Moore, M. Hancher, S. A. Turubanova, A. Tyukavina, D. Thau, S. V. Stehman, S. J. Goetz, T. R. Loveland, A. Kommareddy, A. Egorov, L. Chini, C. O. Justice, J. R. G. Townshend, High-Resolution Global Maps of 21st-Century Forest

Cover Change, Science 342 (2013) 850–853. doi:10.1126/science.1244693.

[128] U. Schneider, A. Becker, P. Finger, A. Meyer-Christoffer, B. Rudolf, M. Ziese, GPCC full data reanalysis version 7.0: Monthly land-surface precipitation from rain gauges built on GTS based and historic data (2016).

[129] T. Fuchs, J. Rapp, F. Rubel, B. Rudolf, Correction of synoptic precipitation observations due to systematic measuring errors with special regard to precipitation phases, Physics and Chemistry of the Earth, Part B: Hydrology, Oceans and Atmosphere 26 (2001) 689–693. doi:10.1016/S1464-1909(01)00070-3.

[130] G. C. Hurtt, L. P. Chini, S. Frolking, R. A. Betts, J. Feddema, G. Fischer, J. P. Fisk, K. Hibbard, R. A. Houghton, A. Janetos, C. D. Jones, G. Kindermann, T. Kinoshita, K. Klein Goldewijk, K. Riahi, E. Shevliakova, S. Smith, E. Stehfest, A. Thomson, P. Thornton, D. P. van Vuuren, Y. P. Wang, Harmonization of land-use scenarios for the period 1500–2100: 600 years of global gridded annual land-use transitions, wood harvest, and resulting secondary lands, Climatic Change 109 (2011) 117–161. doi:10.1007/s10584-011-0153-2.

[131] K. L. Fornace, K. A. Hughen, T. M. Shanahan, S. C. Fritz, P. A. Baker, S. P. Sylva, A 60,000-year record of hydrologic variability in the Central Andes from the hydrogen isotopic composition of leaf waxes in Lake Titicaca sediments, Earth and Planetary Science Letters 408 (2014) 263–271. doi:10.1016/j.epsl.2014.10.024.

[132] M. B. de Toledo, M. B. Bush, Vegetation and hydrology changes in Eastern Amazonia inferred from a pollen record, Anais da Academia Brasileira de Ciências 80 (2008) 191–203. doi:10.1590/S0001-37652008000100014.

[133] M. Zanon, B. A. S. Davis, L. Marquer, S. Brewer, J. O. Kaplan, European Forest Cover During the Past 12,000 Years: A Palynological Reconstruction Based on Modern Analogs and Remote Sensing, Frontiers in Plant Science 9 (2018) 253. doi:10.3389/fpls.2018.00253.

[134] D. Osmont, M. Sigl, A. Eichler, T. M. Jenk, M. Schwikowski, A Holocene black carbon ice-core record of biomass burning in the Amazon Basin from Illimani, Bolivia, Climate of the Past 15 (2019) 579–592. doi:10.5194/cp-15-579-2019.

[135] S. O. Brugger, E. Gobet, D. Osmont, H. Behling, S. L. Fontana, H. Hooghiemstra, C. Morales-Molino, M. Sigl, M. Schwikowski, W. Tinner, Tropical Andean glacier reveals colonial legacy in modern mountain ecosystems, Quaternary Science Reviews 220 (2019) 1–13. doi:10.1016/j.quascirev.2019.06.032.

[136] L. F. Prado, I. Wainer, C. M. Chiessi, Mid-Holocene PMIP3/CMIP5 model results: Intercomparison for the South American Monsoon System, The Holocene 23 (2013) 1915–1920. doi:10.1177/0959683613505336.

[137] I. M. Venancio, S. Mulitza, A. Govin, T. P. Santos, D. O. Lessa, A. L. S. Albuquerque, C. M. Chiessi, R. Tiedemann, M. Vahlenkamp, T. Bickert, M. Schulz, Millennial- to Orbital-Scale Responses of Western Equatorial Atlantic Thermocline Depth to Changes in the Trade Wind System Since the Last Interglacial, Paleoceanography and Paleoclimatology 33 (2018) 1490–1507. doi:10.1029/2018PA003437.

[138] M. A. Maslin, V. J. Ettwein, C. S. Boot, J. Bendle, R. D. Pancost, Amazon Fan biomarker evidence against the Pleistocene rainforest refuge hypothesis?, Journal of Quaternary Science 27 (2012) 451–460. doi:10.1002/jqs.1567.

[139] E. Montoya, U. Lombardo, C. Levis, G. A. Aymard, F. E. Mayle, Human Contribution to Amazonian Plant Diversity: Legacy of Pre-Columbian Land Use in Modern Plant Communities, in: V. Rull, A. C. Carnaval (Eds.), Neotropical Diversification: Patterns and Processes, Springer International Publishing, Cham, 2020, pp. 495–520. doi:10.1007/978-3-030-31167-4_19.

[140] J. Scheff, D. M. W. Frierson, Scaling potential evapotranspiration with greenhouse warming, Journal of Climate 27 (2014) 1539–1558. doi:10.1175/JCLI-D-13-00233.1.

[141] P. K. Panday, M. T. Coe, M. N. Macedo, P. Lefebvre, A. D. d. A. Castanho, Deforestation offsets water balance changes due to climate variability in the Xingu River in eastern Amazonia, Journal of Hydrology 523 (2015) 822–829. doi:10.1016/j.jhydrol.2015.02.018.

[142] M. T. Coe, E. M. Latrubesse, M. E. Ferreira, M. L. Amsler, The effects of deforestation and climate variability on the streamflow of the Araguaia River, Brazil, Biogeochemistry 105 (2011) 119–131. doi:10.1007/s10533-011-9582-2.

[143] M. H. Costa, A. Botta, J. A. Cardille, Effects of large-scale changes in land cover on the discharge of the Tocantins River, Southeastern Amazonia, Journal of Hydrology 283 (2003) 206–217. doi:10.1016/S0022-1694(03)00267-1.

[144] S. J. Hayhoe, C. Neill, S. Porder, R. Mchorney, P. Lefebvre, M. T. Coe, H. Elsenbeer, A. V. Krusche, Conversion to soy on the Amazonian agricultural frontier increases streamflow without affecting stormflow dynamics: CONVERSION TO SOY ON THE AMAZONIAN AGRICULTURAL FRONTIER, Global Change Biology 17 (2011) 1821–1833. doi:10.1111/j.1365-2486.2011.02392.x.

[145] P. W. M. Souza-Filho, E. B. de Souza, R. O. Silva Júnior, W. R. Nascimento, B. R. Versiani de Mendonça, J. T. F. Guimarães, R. Dall'Agnol, J. O. Siqueira, Four decades of land-cover, land-use and hydroclimatology changes in the Itacaiúnas River watershed, southeastern Amazon, Journal of Environmental Management 167 (2016) 175–184. doi:10.1016/j.jenvman.2015.11.039.

[146] S. A. Cowling, Y. Shin, Simulated ecosystem threshold responses to co-varying temperature, precipitation and atmospheric CO2 within a region of Amazonia, Global Ecology and Biogeography 15 (2006) 553–566.

[147] B. M. Flores, M. Holmgren, C. Xu, E. H. van Nes, C. C. Jakovac, R. C. G. Mesquita, M. Scheffer, Floodplains as an Achilles' heel of Amazonian forest resilience, Proceedings of the National Academy of Sciences 114 (2017) 4442–4446. doi:10.1073/pnas.1617988114.

[148] D. Galbraith, P. E. Levy, S. Sitch, C. Huntingford, P. Cox, M. Williams, P. Meir, Multiple mechanisms of Amazonian forest biomass losses in three dynamic global vegetation models under climate change, New Phytologist 187 (2010) 647–665. doi:10.1111/j.1469-8137.2010.03350.x.